

**MEASUREMENT OF CEREBRAL PERFUSION IN
PARKINSON'S DISEASE WITH MILD COGNITIVE
IMPAIRMENT USING ARTERIAL SPIN LABELING MRI**

by

Dilek Betül ARSLAN

B.Sc., Biomedical Engineering, Erciyes University, 2013

Submitted to the Institute of Biomedical Engineering
in partial fulfillment of the requirements
for the degree of
Master of Science
in
Biomedical Engineering

Boğaziçi University

2016

**MEASUREMENT OF CEREBRAL PERFUSION IN
PARKINSON'S DISEASE WITH MILD COGNITIVE
IMPAIRMENT USING ARTERIAL SPIN LABELING MRI**

APPROVED BY:

Assist. Prof. Dr. Esin Öztürk Işık
(Thesis Advisor)

Prof. Dr. Cengizhan Öztürk

Prof. Dr. Tamer Demiralp

DATE OF APPROVAL: 25 July 2016

ACKNOWLEDGEMENTS

I am grateful to my advisor, Assist. Prof. Dr. Esin Öztürk Işık , for understanding, generous guidance and support. It has been a pleasure working with her. Furthermore, I would like to thank my thesis committee, Prof. Dr. Cengizhan Öztürk and Prof. Dr. Tamer Demiralp, for their encouragement and valuable suggestions.

I would like to thank a lot to my colleagues, Sevim Cengiz, Gökçe Hale Hatay, Ani Kıçık and Emel Erdoğan, for their guidance and friendship. I'm also thankful to my parents for their support.

This study was supported by TÜBİTAK project #115S219 and the Ministry of Development project #2010K120330

ACADEMIC ETHICS AND INTEGRITY STATEMENT

I, Dilek Betül Arslan, hereby certify that I am aware of the Academic Ethics and Integrity Policy issued by the Council of Higher (YÖK) and I fully acknowledge all the consequences due to its violation by plagiarism or any other way.

Name :

Signature:

Date:

ABSTRACT

MEASUREMENT OF CEREBRAL PERFUSION IN PARKINSON'S DISEASE WITH MILD COGNITIVE IMPAIRMENT USING ARTERIAL SPIN LABELING MRI

Mild cognitive impairment is a common symptom of Parkinson's disease (PD). Objective imaging biomarkers are required for the diagnosis of PD with mild cognitive impairment (PD-MCI). Arterial spin labeling MRI (ASL-MRI) enables the measurement of cerebral blood flow (CBF) without using contrast agent or ionizing radiation. In this study, ASL-MR images of 19 PD-MCI and 19 cognitively normal PD (PD-CN) patients were acquired at 3T. CBF maps were calculated with arterial blood volume (aBV) correction using the quantitative imaging of perfusion using a single subtraction (QUIPSS II) formula. CBF and aBV maps were fused into T2 weighted (T2w) MR images, and registered to MNI152 brain atlas in FSL. The CBF and aBV values of several brain regions were compared between PD-MCI and PD-CN patients. The differences in histogram parameters of CBF maps, which were estimated with and without aBV correction, were assessed. The correlations between the neuropsychological test scores and CBF values were assessed. The CBF values in different brain regions of each group were compared with each other. A graphical user interface (GUI) was designed in order to calculate CBF maps out of ASL-MRI in MATLAB. There were not any statistically significant differences between the CBF values of PD-MCI and PD-CN patients. There were some variations between the CBF values of the brain regions in PD-MCI and PD-CN groups. There was a trend of a negative correlation between the neuropsychological test scores and the CBF values in some brain regions of PD-MCI patients. The results of this study combined with other MR parameters might enable the definition of an MR based biomarker for PD-MCI diagnosis.

Keywords: Arterial spin labeling, Parkinson's disease, mild cognitive impairment, QUIPSS II, cerebral blood flow.

ÖZET

HAFIF KOGNİTİF BOZUKLUĞU OLAN PARKİNSON HASTALIĞINDA SEREBRAL PERFÜZYONUN ATARDAMAR FIRIL ETİKETLEME MRG KULLANILARAK ÖLÇÜMÜ

Hafif kognitif bozukluk, Parkinson hastalığının (PH) yaygın bir belirtisidir. Parkinson hastalığında hafif kognitif bozukluk (PH-HKB) tanısında kullanılacak nesnel görüntüleme biyoişaretleyicileri gerekmektedir. Atardamar fırıl etiketleme MRG (ASL-MRG) kontrast madde ya da iyonlaştırıcı radyasyon kullanmadan serebral kan akışını (SKA) ölçmeyi sağlamaktadır. Bu çalışmada, 19 PH-HKB ve 19 işlevsel normal Parkinson hastasında (PH-KN) ASL-MR görüntüleri, 3T manyetik alanda alındı. SKA haritaları perfüzyonün tek çıkarım ile kantitatif görüntülenmesi (QUIPSS II) formülü kullanılarak atardamar kan hacmi (aKH) düzeltilmesi ile hesaplandı. SKA ve aKH haritaları FSL'de T2 ağırlıklı MR görüntülerinin içine yerleştirilerek birleştirildi ve MNI152 beyin atlasıyla karşılaştırıldı. PH-HKB ve PH-KN hastaları arasında çeşitli beyin bölgelerinin SKA ve aKH değerleri karşılaştırıldı. aKH düzeltilmesi yapılarak ve yapılmayarak hesaplanan SKA haritalarının histogram parametrelerindeki farklılıklar değerlendirildi. Nöropsikolojik test skorları ve SKA değerleri arasındaki korelasyonlar değerlendirildi. Her grubun farklı beyin bölgelerindeki SKA değerleri birbirleriyle karşılaştırıldı. Bir grafiksel kullanıcı arayüzü ASL-MRG'den SKA değerlerini hesaplamak için MATLAB'de tasarlandı. PH-HKB ve PH-KN hastaların SKA değerleri arasında istatistiksel olarak anlamlı fark yoktu. PH-HKB ve PH-KN gruplarının beyin bölgelerindeki SKA değerleri arasında bazı varyasyonlar vardı. PH-HKB hastalarının bazı beyin bölgelerinde SKA değerleri ile nöropsikolojik test skorları arasında negatif bir korelasyon eğilimi vardı. Bu çalışmanın sonuçlarının diğer MR parametreleri ile birleştirilmesiyle PH-HKB tanısı için MR temelli bir biyoişaretleyicinin tanımlanması mümkün olabilir.

Anahtar Sözcükler: Atardamar fırıl etiketleme, Parkinson hastalığı, hafif kognitif bozukluk, QUIPSS II, serebral kan akışı

TABLE OF CONTENTS

ACKNOWLEDGEMENTS	iii
ACADEMIC ETHICS AND INTEGRITY STATEMENT	iv
ABSTRACT	v
ÖZET	vi
LIST OF FIGURES	ix
LIST OF TABLES	xi
LIST OF SYMBOLS	xii
LIST OF ABBREVIATIONS	xiii
1. INTRODUCTION	1
2. BACKGROUND	4
2.1 Parkinson’s Disease	4
2.1.1 Parkinson’s Disease Causes	4
2.1.2 Diagnosis	5
2.1.3 Clinical Manifestations	5
2.1.3.1 Motor Symptoms	5
2.1.3.2 Nonmotor Symptoms	6
2.1.4 Cognitive Impairment in PD	6
2.2 Cerebral Blood Flow	6
2.3 Arterial Spin Labeling MRI	8
2.3.1 ASL-MRI Principles	8
2.3.2 ASL Labeling Techniques	9
2.3.2.1 Continuous Arterial Spin Labeling	9
2.3.2.2 Pulsed Arterial Spin Labeling	10
2.3.2.3 Pseudo-Continuous Arterial Spin Labeling	12
2.3.3 ASL-MRI Artifacts	12
2.4 Readout	14
2.4.1 Look-Locker	14
2.5 ASL-MRI Models of Quantification	15
2.5.1 Single Compartment Analysis	15

2.5.2	General Kinetic Model	17
2.5.2.1	QUIPSS II	19
2.5.2.2	QUASAR	20
2.6	Literature Review	23
3.	MATERIALS and METHODS	25
3.1	Subjects	25
3.2	Diagnostic Criteria and Assessment	25
3.2.1	Assessment of Cognitive Impairment	26
3.2.1.1	Stroop Test	26
3.2.1.2	The Wisconsin Card Sorting Test	27
3.2.1.3	The Benton Judgment of Line Orientation Test	27
3.2.1.4	The Symbol Digit Modalities Test	28
3.2.1.5	The Addenbrooke's Cognitive Examination Revised	28
3.3	Data Acquisition	28
3.4	Data Processing and Analysis	31
3.4.1	CBF and aBV Map Calculation	31
3.4.2	Registration to MNI152 Brain Atlas	32
3.4.3	Histogram Analysis	33
3.4.4	Graphical User Interface Design	34
3.4.5	Statistical Analysis	35
4.	RESULTS	38
4.1	The CBF and aBV Values	38
4.2	The Mean CBF Value Differences	43
4.3	Correlation of Neuropsychological Test Scores and CBF Values	45
4.4	Histogram	48
5.	DISCUSSION	50
6.	CONCLUSION	53
	APPENDIX A. Software Packages	54
	REFERENCES	55

LIST OF FIGURES

Figure 2.1	The relationship between $h(\tau)$ and $R(t)$.	8
Figure 2.2	Inversion profiles of tag and control pulses for EPISTAR [22].	10
Figure 2.3	Inversion profiles of tag and control pulses for FAIR [22].	11
Figure 2.4	Inversion profiles of tag and control pulses for PICORE [22].	11
Figure 2.5	Susceptibility artifact of an EPI readout.	12
Figure 2.6	Motion artifact.	13
Figure 2.7	Parallel imaging artifact.	13
Figure 2.8	A QUASAR sequence diagram [6].	22
Figure 3.1	T2-weighted MR image.	29
Figure 3.2	Pulse sequence diagram of ASL-MRI in Philips Achieva 3T scanners.	30
Figure 3.3	The demonstration of slices at different TIs.	30
Figure 3.4	The subtraction of control and tag images.	31
Figure 3.5	Masking in a control image. a) Control image at a given slice, b) masked out tissue, and c) masked control image of the slice.	31
Figure 3.6	T2w MR image of a subject after removing skull.	32
Figure 3.7	The FSL view of CBF-T2w MR fused image.	33
Figure 3.8	The FSL view of a CBF-T2w MR incorrectly fused image due to subject motion.	34
Figure 3.9	The FSL view of MNI152 atlas.	35
Figure 3.10	The GUI of CBF map calculation.	37
Figure 4.1	M_0 maps taken from 1 st region of a PD-CN patient.	38
Figure 4.2	M_0 maps taken from the 2 nd region of a PD-CN patient.	39
Figure 4.3	M_0 maps taken from the 3 rd region of a PD-CN patient.	39
Figure 4.4	M_0 fit in a given pixel.	40
Figure 4.5	The CBF map calculated with a constant M_0 .	40
Figure 4.6	The CBF map calculated with real M_0 values.	41
Figure 4.7	CBF maps taken from the 1 st region of a PD-CN patient.	41
Figure 4.8	CBF maps taken from the 2 nd region of a PD-CN patient.	42

Figure 4.9	CBF maps taken from the 3 rd region of a PD-CN patient.	42
Figure 4.10	aBV maps taken from the 1 st region of a PD-CN patient.	43
Figure 4.11	The histogram of a CBF map calculated without aBV correction.	48
Figure 4.12	The histogram of a CBF map calculated with aBV correction.	49



LIST OF TABLES

Table 3.1	Demographics of patients.	25
Table 4.1	The mean CBF values (\pm std) of PD-CN and PD-MCI patients in different brain regions, and the p-values calculated with a Mann-Whitney ranksum test.	44
Table 4.2	The mean aBV values (\pm std) of PD-CN and PD-MCI patients in different brain regions, and the p values calculated with a Mann-Whitney ranksum test.	44
Table 4.3	The mean rank of CBF values in some brain regions, and p values calculated with a Friedman test.	45
Table 4.4	Neuropsychological test scores of PD-MCI and PD-CN patients.	46
Table 4.5	The mean test scores values (\pm std) of PD-CN and PD-MCI, and p values calculated with a Mann-Whitney ranksum test.	46
Table 4.6	The mean test scores (\pm std) in different brain regions, and p values calculated with Spearman rank correlation test.	47
Table 4.7	The histogram analysis of patients in one brain slice, and p values calculated with Wilcoxon signed rank test.	48

LIST OF SYMBOLS

aBV	Arterial blood volume fraction
AIF	Arterial input function
$c(t)$	Normalized arterial concentration of magnetization
f	Brain blood flow
$h(\tau)$	Distribution function of tracers
$R(t)$	Residue function
TI_1	Time of application of the saturation pulse in the imaging slice
T_{1b}	Longitudinal relaxation time of blood
T_{1eff}	Effective longitudinal relaxation time
T_{1t}	Longitudinal relaxation time of tissue
T_{ex}	Exchange time
TI	Inversion time
TI_2	Time of acquisition image
M_0	Magnetization under fully relaxed conditions
$M_a t$	Longitudinal magnetization per ml of arterial blood
$M_b t$	Longitudinal magnetization per gram of brain tissue
q_0	Quantity of labeled blood in beginning
q	Correction factor
$q(t)$	Total amount of remaining tagged blood in brain
ΔM	Net magnetization
Δta	Bolus arrival time
ΔTI	Time between the RF pulses
α	Labeling efficiency
λ	Blood brain partition coefficient of water
τ	Time width of the tag
τa	Bolus duration of the arterial bolus
δt	Transit time of blood from the tagging region to the imaging slice

LIST OF ABBREVIATIONS

3D	Three-dimensional
ACER	Addenbrooke's Cognitive Examination Revised
aBV	Arterial Blood Volume
AD	Alzheimer's Disease
ASL	Arterial Spin Labeling
BAT	Bolus Arrival Time
CASL	Continuous Arterial Spin Labeling
CBF	Cerebral Blood Flow
DTI	Diffusion Tensor Imaging
EPI	Echo Planar Imaging
EV	Extravascular
FAIR	Flow Sensitive Alternating Inversion Recovery
FE	Frequency Encoding
FOV	Field Of View
FSL	FMRIB Software Library
HC	Healthy Control
GRAPPA	Generalized Auto Calibrating Partially Parallel Acquisition
GUI	Graphical User Interface
IV	Intravascular
LL	Look-Locker
MMSE	Mini-Mental State Examination
MNI	Montreal Neurological Institute
MR	Magnetic Resonance
MRI	Magnetic Resonance Imaging
MT	Magnetization Transfer
PASL	Continuous Arterial Spin Labeling
PCASL	Pseudo Continuous Arterial Spin Labeling
PD	Parkinson's Disease

PD-CN	Parkinson's Disease with Cognitively Normal
PDD	Parkinson's Disease with Dementia
PD-MCI	Parkinson's Disease with Mild Cognitive Impairment
PE	Phase Encoding
PET	Positron Emission Tomography
PI	Parallel Imaging
PICORE	Proximal Inversion with Control of Off-Resonance Effects
PULSAR	Pulsed Star Labeling of Arterial Regions
SAR	Specific Absorption Rate
SPECT	Single Photon Emission Computerized Tomography
STAR	Signal Targeting with Alternating Radiofrequency
SENSE	Sensitivity Encoding
STD	Standard Deviation
SDMT	Symbol Digit Modalities Test
SNK	Student-Newman-Keuls
SNR	Signal to Noise Ratio
RF	Radio Frequency
ROI	Region of Interest
TI	Inversion Time
TE	Echo Time
TR	Repetition Time
UPDRS	Unified Parkinson Disease Rating Scale
QUASAR	Quantitative Star Labeling of Arterial Region
QUIPSS	Quantitative Imaging of Perfusion Using a Single Subtraction
WCST	Wisconsin Card Sorting Test

1. INTRODUCTION

Parkinson's disease (PD) is a progressive disorder that worsens with time. The decline happens slowly in most people. In general, PD has been known as a movement disorder. Also, it has been characterized by certain symptoms such as tremor and slowness of movement. However, it is a fact that it has nonmotor symptoms including cognitive difficulties. At the beginning, patients diagnosed with PD are cognitively normal. During the course of the disease, patients undergo mild cognitive impairment and, eventually, some evolve into dementia. Mild cognitive impairment is a common sign of non-demented Parkinson's disease. PD with mild cognitive impairment (PD-MCI) is currently diagnosed on the basis of clinical and neuropsychological tests. Because many factors could affect the results of these tests, investigators have focused on neuroimaging techniques to develop and identify alternative measures of disease status and progression [1]. However, there is still a need for objective imaging biomarkers in order to diagnose PD. And, this need provides the impetus for this thesis.

Perfusion is described as the volume of blood delivered to capillary beds per unit volume of brain tissue per unit time. Cerebral blood flow (CBF) can be directly related to neural activity and regional metabolism. Thus, it is a remarkable parameter of neural activity in cognitive and clinical neuroscience studies. Arterial spin labeling magnetic resonance imaging (ASL-MRI) enables cerebral blood flow measurement. This technique has advantages compared to other perfusion MR techniques. One important advantage of this technique is not to use any contrast agent or ionizing radiation. On the contrary, this technique has the disadvantage of low signal-to-noise ratio (SNR). In ASL-MRI, there are two experiments including control and tag. In tag experiment, protons within arterial blood are magnetically tagged before entering the tissue of interest at the neck level by applying a 180° radiofrequency (RF) pulse that inverts the net magnetization of the blood water. The tagged blood passes into brain tissue, after a time delay, called inversion time (TI), in ASL-MRI. At time TI after the pulsed labeling, the images are acquired with a rapid imaging technique. These images

are called 'tag images'. In control experiment, protons within arterial blood aren't inverted. The control images are acquired in the region of interest. The control and the tag images are subtracted to create a perfusion-weighted MR image, which shows the amount of arterial blood delivered to each voxel within the slice within the transit time. There are three main ASL techniques, which are continuous arterial spin labeling (CASL), pulsed arterial spin labeling (PASL) and pulsed continuous arterial spin labeling (PCASL) [2]. Readout techniques have been developed for ASL. By and large, echo planar imaging (EPI) readout is used in clinical and research centers. The other common readout is Look-Locker. This readout is combined with EPI. This readout consists of one inversion pulse and several pulses with a low flip angle. In ASL-MRI images, a few artifacts are commonly seen. These artifacts include geometric distortion of EPI readout, motion artifacts, and parallel imaging (PI) artifacts. The recognition of these artifacts is important, because it can be critical in interpretation of the CBF maps. Quantification models of ASL are based on single compartment analysis developed by Williams et al. [3] and general kinetic model developed by Buxton et. al. [4]. In single compartment analysis, Bloch equation is applied. General kinetic model has 3 functions including arterial input function, residue function, and relaxation function. This model is described as mathematical formulas of the dynamic tissue concentration of any tracer delivered to the tissue by blood flow. General kinetic model has been modified as the quantitative imaging of perfusion using a single subtraction (QUIPSS) I and II [5] and quantitative star labeling of arterial region (QUASAR) [6]. In QUIPSS, there are pre- and post- saturation pulses in order to eliminate variable transit delays occurring when images are acquired before tagged blood flows into the imaging slice. In QUASAR, STAR labeling is combined with Look-Locker readout and QUIPSS II. There are also bipolar gradients in order to eliminate microvascular signal.

Previous studies using ASL-MRI for CBF quantification have reported reduced perfusion in post cingulate gyrus, precuneus, cuneus and sub-frontal gyrus. These studies compared CBF values of PD-MCI, PD-CN and PD with dementia (PDD) patients or healthy controls (HC) by using ASL-MRI. Only, one of these studies employed multi-TI ASL-MRI and the other studies used single TI, which has been reported to provide less reliable CBF measurements than ASL-MRI with multi TI [7, 8, 9, 10].

There is a need for defining objective imaging biomarkers to characterize cognitive status and progression in PD. The main purpose of this thesis was to define possible brain perfusion based biomarkers that would help in PD-MCI diagnosis.



2. BACKGROUND

2.1 Parkinson's Disease

Following Alzheimer's disease, PD is the second most common neurodegenerative disorder at present. PD is related to debilitating motor symptoms. Also, PD causes a reduction of life expectancy. The risk of PD increases with age. In today's aging population, the number of individuals suffering from PD increase, which brings substantial personal, social, and economic burdens [11]. James Parkinson first described PD in his publication called "An Essay on the Shaking Palsy" [12]. This publication was based on his observations of six patients with PD. Later, alternative names such as 'PD', 'Paralysis agitans' and 'Shaking palsy' were suggested for PD. Afterwards, Charcot realized the importance of PD and suggested that this disorder would bear James Parkinson's name.

2.1.1 Parkinson's Disease Causes

What causes PD has not been fully understood, and the symptoms and results of PD might vary from person to person. There are nerve cells producing dopamine in the brain. Dopamine, which is a chemical messenger, is responsible for transmitting signals between the substantia nigra and multiple brain regions, which provides the control and coordination of body movements. If these nerve cells become impaired or die, the amount of dopamine decreases in the brain. As a result of this, movements become slow and abnormal. The loss of these nerve cells may result from a combination of genetic and environmental factors [13].

In the majority of PD cases, non-genetic factors play a remarkable role. Exposure to toxins and heavy metals increases the the PD development, whereas coffee consumption decreases it. Also, it is reported that smoking has an inverse association

with PD. Furthermore, bad dietary habits might contribute to a higher risk of PD [13]. In a small group of PD cases, gene mutations can directly cause PD. These mutations induce the decrease of dopamine. If a person's parents have PD, he or she is at a higher risk of developing PD than other people whose patients don't have PD [13].

2.1.2 Diagnosis

Diagnosis is important in order to monitor status and progression of PD. However, diagnosis of PD is complicated. Furthermore, it may take some time to diagnose PD. The symptoms are combined with some tests for an accurate diagnosis. The common tests used for PD diagnosis are The Hoehn and Yahr Scale and The Unified Parkinson's Disease Rating Scale (UPDRS). Rigidity, postural deformities, tremor and bradykinesia are main manifestations of PD. Also, diagnosis of PD is based on medical history [14].

2.1.3 Clinical Manifestations

PD has certain motor symptoms including tremor, rigidity, gait and posture disturbances. Also, it has non-motor symptoms such as cognitive impairment and dementia. It may be possible to diagnose PD in the early stages, because some of the non-motor symptoms of PD may be apparent before any of the motor symptoms emerge. So, identifying non-motor symptoms is important [14].

2.1.3.1 Motor Symptoms

PD affects not only the brain but also the body movements. Motor symptoms begin manifesting in PD when 50-70% of the cells in the substantia nigra have already been lost [15]. One of the main symptoms is tremor at rest, which is the most visible hallmark of PD. Two important motor symptoms are rigidity and bradykinesia meaning

"slow movement". Another one of the most important signs of Parkinson's disease is postural instability. Also, many patients experience speech impairments [14].

2.1.3.2 Nonmotor Symptoms

Nonmotor symptoms are defined as neuropsychiatric disturbances. Some of these symptoms are autonomic dysfunctions, such as orthostatic hypotension, urinary frequency, constipation and profuse sweating. The others neuropsychiatric disturbances include cognitive/neurobehavioral disorders, and sensory and sleep abnormalities. These symptoms aren't enough to define PD, but these markers are conducive to better understand the disease process [14].

2.1.4 Cognitive Impairment in PD

Common and remarkable features of PD are cognitive impairments and dementia. In PD patients without dementia, cognitive deficits occur frequently (up to approximately 50%) in the early stages of the disease. Mild cognitive impairment (MCI) is a degree of cognitive decline that isn't usually related to age. MCI differs from dementia. Unlike dementia, the changes resulted from MCI are not severe enough to affect activities of daily life and normal social function. MCI is an intermediate state between normal cognitive function and dementia in PD. PD-MCI has an increased risk for developing dementia. Presence of mild cognitive dysfunction in PD is seen in many cases from early stages. Thus, identification of MCI is significant. However, diagnosis of MCI in PD is usually complex and remains challenging [16].

2.2 Cerebral Blood Flow

The brain receives its blood supply from four main arteries. These are the two internal carotid arteries and the two vertebral arteries. Adequate blood flow in brain

is significant for not only the supply of oxygen and nutrients, but also the removal of waste from tissue. Therefore, measurement of blood flow, called cerebral blood flow (CBF), is important for the assessment of tissue viability and function. CBF is a quantifiable physiological parameter, and is related to neuronal metabolism, which provides information for neurological disorders. CBF is presented in units of milliliters of blood per 100 g of brain tissue per minute (ml/g/min). It has been reported that the CBF value ranges from 40 to 100 ml/100 g/min [17, 18].

In principle, measurement of CBF is based on the "indicator-dilution" theory. The indicator dilution theory describes the passage of a tracer through the brain. The indicator particles follow different paths and the amount of these particles decreases in time. The transport function, $h(\tau)$, is the distribution function of tracers which has left the brain in a while. Total fraction of tracer is equal to one [19]. Therefore, the integral of transport function over time equals unity, which can be represented as,

$$\int_0^{\infty} h(\tau) d\tau = 1. \quad (2.1)$$

The residue function, $R(t)$, is defined as the fraction of tracer still present in the brain at time t after bolus injection, and can be represented as,

$$R(t) = 1 - \int_0^t h(\tau) d\tau. \quad (2.2)$$

Therefore, $R(t)$ and $h(\tau)$ are important hallmarks for the system and Figure 2.1 displays the relationship between $R(t)$ and $h(\tau)$. There have been many techniques including positron emission tomography (PET) and single-photon emission computed tomography (SPECT) in order to quantify CBF. By and large, these techniques are based on monitoring tracer injections. Firstly, some substance that can be detected easily gets injected in the blood. Afterwards, the concentration of the tracer is measured by means of an appropriate detector while the tracer travels through the brain [17].

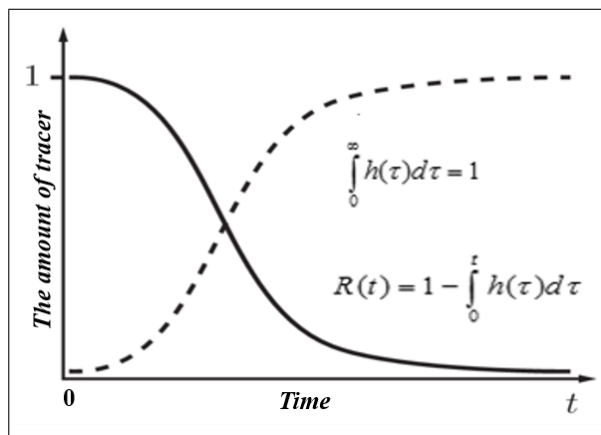


Figure 2.1 The relationship between $h(\tau)$ and $R(t)$.

2.3 Arterial Spin Labeling MRI

ASL-MRI is one of the magnetic resonance imaging techniques that can be used to measure CBF. There are advantages and disadvantages of ASL-MRI in comparison to other techniques. ASL-MRI is a noninvasive method. Therefore, it is repeatable at multi times, which enables to track relative changes in CBF easily. ASL-MRI doesn't use any contrast agents that can be potentially harmful. As a result of this, it doesn't adversely affect patient health [3]. Another advantage of ASL-MRI is generating CBF images with higher spatial and temporal resolution than some other current techniques [20]. Even though ASL-MRI has several advantages, ASL-MRI has low signal-to-noise ratio, which might adversely affect the quantification of CBF [3].

2.3.1 ASL-MRI Principles

At the neck vessels, protons in arterial blood are magnetically tagged by applying a 180° RF pulse that inverts the net magnetization of the blood water. Tagged blood acts as a magnetic tracer. The tagged protons are then carried by means of the arterial vessels towards the brain tissue where they pass from the capillary compartment to the extra vascular compartment. The tagged blood passes into brain tissue. After some TI, the ASL-MR images are acquired with a rapid imaging technique. These images are called the 'tag' images. This experiment is then repeated

without magnetically tagging water molecules within arterial blood to yield another set of images, which are called the 'control' images. In tag images, the magnetization of arterial blood is inverted. On the other hand, the magnetization of arterial blood is fully relaxed in control images. The control image and the tag image are subtracted to create a perfusion-weighted image, which shows the amount of arterial blood delivered to each voxel within the slice within the transit time. Subtraction of labeled images from control images eliminates static tissue signal. The remaining signal is a relative measure of perfusion proportional to CBF [3].

2.3.2 ASL Labeling Techniques

There are three main types of proton labeling in ASL, which are continuous arterial spin labeling (CASL), pulsed arterial spin labeling (PASL), and pseudo-continuous arterial spin labeling (PCASL). ASL-MRI is categorized in terms of proton labeling type.

2.3.2.1 Continuous Arterial Spin Labeling

CASL uses long and continuous RF pulses, with slice-selective gradients. CASL has advantages, one of which is to provide a higher SNR than other ASL-MRI techniques, such as PASL. In addition to this, CASL provides higher perfusion contrast than other types of labeling. However, it has several drawbacks. The long inversion pulses brings about magnetization transfer (MT) effects and cause the person to be exposed to large amount of RF energy, which increases specific absorption rate (SAR) [21].

2.3.2.2 Pulsed Arterial Spin Labeling

Unlike CASL, PASL uses short RF pulses. Inversion of the arterial blood occurs over a specific area which is known as a tagging region. Short RF pulses induce less MT effects with respect to CASL. The disadvantage of this technique is the imperfect edges of the tag pulses. Therefore, a spatial gap between the distal edge of the tagging slab and imaging plane is required. Several techniques have been developed for PASL. The difference among these methods is the place of the tagging plane and the choice of how the blood is tagged magnetically for the control and label images [21].

One of these PASL techniques is Echo Planar Imaging and Signal Targeting with Alternating Radiofrequency (EPISTAR). This technique was first proposed by Edelman et al. in 1994. Tagging is applied in a slab below the imaging slice, while inversion in control experiments is performed in a slab symmetrically above the imaging slice. This sequence was originally a single slice technique. Multislice acquisition was achieved by using single inversion pulse for the label experiment and two half 180° RF pulses for the control experiment at the same proximal location in order to compensate for MT effects [22].

Since this technique has balanced slice selection gradients for control and tag experiments, it could have fewer eddy current artifacts [2]. Figure 2.2 shows the magnetization after RF pulses are applied for control and tag experiments in EPISTAR technique for a single slice. Another PASL technique is Flow Sensitive Alternating

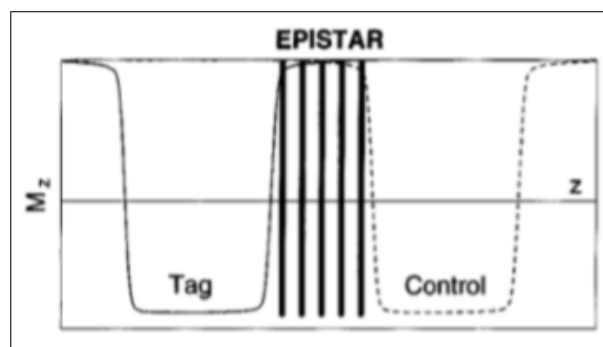


Figure 2.2 Inversion profiles of tag and control pulses for EPISTAR [22].

Inversion Recovery (FAIR). Arterial blood is tagged by using non selective inversion, which means that everything within RF coil is inverted. The imaging slice is also affected. Control image is acquired after a selective inversion. This sequence minimizes MT effects [23]. In FAIR technique, slice profile is thinner with respect to EPISTAR and Proximal Inversion with Control of Off-Resonance Effects (PICORE). So, the profile of the edge of the tag is sharper, which is conducive to correctly quantify CBF maps [2]. Figure 2.3 shows the tag and control planes for FAIR technique. Another PASL

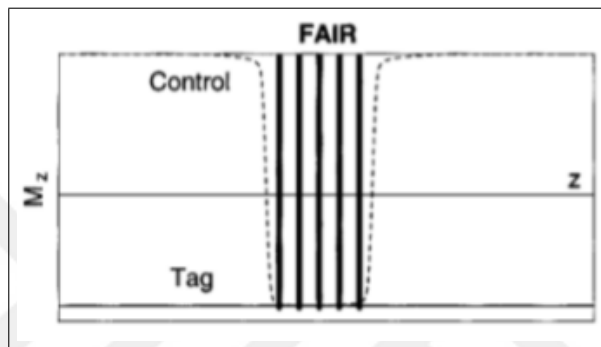


Figure 2.3 Inversion profiles of tag and control pulses for FAIR [22].

technique is PICORE. Tag method is the same in EPISTAR and PICORE. Tagging is applied in a slab below the imaging slice by applying a 180° RF pulse with a selective gradient. In control experiments, off-resonance inversion pulses are applied without a gradient. That means that nothing in the control plane is inverted. Therefore, the control pulses compensate MT effects, because these pulses don't invert the magnetization of the spins [2]. Figure 2.4 shows that control plane is wider than tag plane in the PICORE technique.

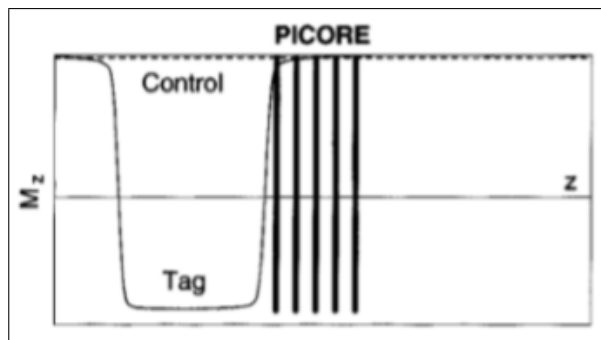


Figure 2.4 Inversion profiles of tag and control pulses for PICORE [22].

2.3.2.3 Pseudo-Continuous Arterial Spin Labeling

PCASL is one of the ASL-MRI techniques. It combines CASL's high SNR and PASL's higher tagging efficiency. Unlike CASL, PCASL compensates for the MT effects. The other advantage of PCASL is less RF power deposition with respect to CASL [21].

2.3.3 ASL-MRI Artifacts

There are several artifacts commonly encountered in ASL-MRI images. Familiarity with these artifacts may prevent errors in the assessment of the CBF maps. One of these artifacts is the susceptibility artifact resulting from the EPI readout. EPI is commonly used in ASL-MRI readout in order to speed up the data acquisition. One disadvantage of EPI is susceptibility, which causes a dark signal in the CBF maps. This artifact can be misinterpreted and might result in a wrong diagnosis [24]. In Figure 2.5, the loss of the signal intensity due to the susceptibility artifact resulting from an EPI readout is shown with a red arrow. Another artifact stems from the motion

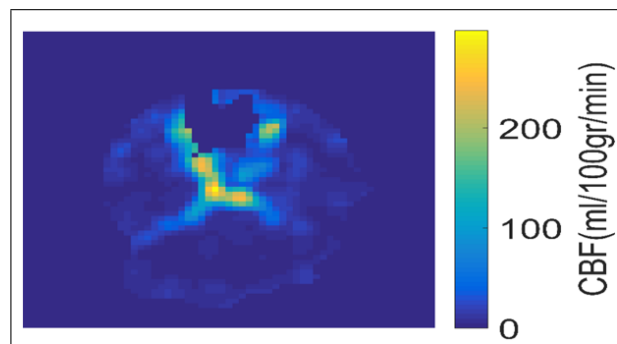


Figure 2.5 Susceptibility artifact of an EPI readout.

of patients. Motion artifact is encountered to a large extent, especially, in hospitals. The pattern of this artifact is a peripheral ring of high signal intensity. Figure 2.6 shows that the top-right peripheral of brain has higher signal intensity with respect to the other brain regions. Also, this ASL-MRI image belongs to a patient diagnosed with glioma, and the high signal intensity resulting due to motion might be confusing

when clinicians evaluate this image. Another artifact is the parallel imaging (PI) ar-

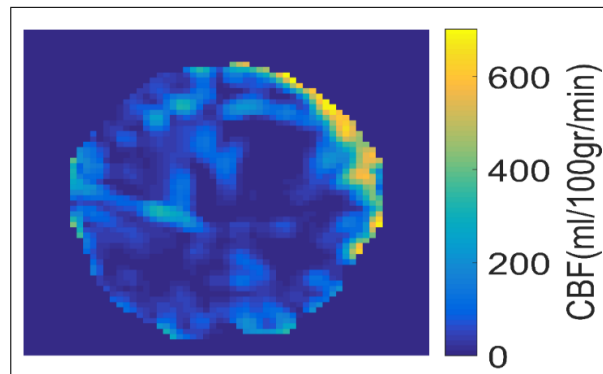


Figure 2.6 Motion artifact.

tifact. Parallel imaging is a technique for rapid acquisition. It exploits the multiple elements of a phased array coil. This artifact is seen due to subtraction in ASL-MRI [25]. Sensitivity encoding (SENSE) [26] and generalized partially parallel acquisitions (GRAPPA) [27] are two common PI techniques. In SENSE, the image is reconstructed in the image domain after Fourier transform. In GRAPPA, the image is reconstructed in the frequency domain before Fourier transform. PI artifact of SENSE technique appears as aliasing, whereas GRAPPA causes a grainy image. Figure 2.7 shows an aliasing artifact due to SENSE [28].

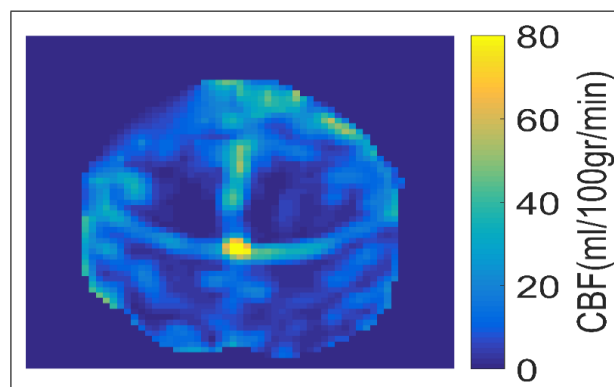


Figure 2.7 Parallel imaging artifact.

2.4 Readout

RF pulses don't provide spatial information. Therefore, gradients are employed. There are three types of gradients, including frequency encoding (FE) gradient, phase encoding (PE) gradient and slice selection (SE) gradient. If SE gradients are applied, RF pulses is restricted in order to select a region of the field of view (FOV). These pulses are described as selective. If no SE gradient is applied, pulses are called non selective [29]. In tag experiments, selective gradients are employed, while non-selective gradients are employed in control experiments.

Several readout techniques have been developed for ASL-MRI in the past. One common technique is EPI consisting of rapid series of gradient echoes so as to cover k-space after a single or multi-excitation pulse. The artifact of this readout is signal loses and geometric distortions. To get rid of these drawbacks, multiple TI protocol is used. The application of multi TI is a conducive way to measure multiple phases of CBF maps. This approach provides more accurate CBF maps. However, the disadvantage of this method is longer data acquisition time. Therefore, parallel imaging techniques can be applied in order to speed up the readout.

2.4.1 Look-Locker

Look-Locker (LL) is one of ASL-MRI readouts in order to speed up multi TI acquisition. Its name originates from its two inventors [30]. It has been combined with EPI readouts. This readout consists of one inversion pulse and several pulses with a low flip angle. EPI readout follows these pulses so as to sample the whole brain. This technique enables higher temporal information without increasing the scan time. However, the application of multiple readout pulses perturbs the recovery of the magnetization. Therefore, the disadvantage of this technique is the low signal amplitude [31]. In 2001, LL readout was combined with a FAIR labeling scheme [32]. Later, Petersen et. al. used STAR labeling with LL readout [6]. But, there is a difficulty with quantification of CBF maps, since LL readout requires a more complex

model for perfusion quantification. In LL, the effective longitudinal relaxation time is defined as,

$$T_{1eff} = \frac{1}{\frac{1}{T_{1b}} - \frac{\log(\cos\alpha)}{\Delta TI}}, \quad (2.3)$$

where, α is the readout flip angle and ΔTI is the time between the RF pulses.

2.5 ASL-MRI Models of Quantification

There are several quantification techniques in order to obtain CBF maps. Firstly, tag and control images are obtained. After that these images are subtracted in order to generate perfusion weighted images. After subtraction, tissue part without blood vessels in brain is eliminated. This process is common in ASL-MRI quantification techniques. How the difference of these images is interpreted is an important parameter for estimation of CBF maps. This interpretation is based on either compartmental modeling or tracer kinetics.

2.5.1 Single Compartment Analysis

Williams et al. introduced the principle of CBF in ASL-MRI by applying the Bloch equations [33]. The model describes the microvasculature and tissue within the imaging slice as a single compartment. It is assumed that water is a freely diffusible tracer with an extraction fraction of 100%. This means that inverted arterial water is instantaneously exchanged with tissue water upon its arrival. Taking into account of tissue perfusion, the longitudinal Bloch equation is given by;

$$\frac{dM(t)}{dt} = \frac{M_0 - M_b(t)}{T_{1t}} + fM_a(t) - f\frac{M_b(t)}{\lambda}, \quad (2.4)$$

where, f is brain blood flow, M_0 is magnetization under fully relaxed conditions, $M_b(t)$ is longitudinal magnetization per g of brain tissue, T_{1t} is spin lattice relaxation time of brain water in the absence of flow, $M_a(t)$ is the longitudinal magnetization per

ml of arterial blood, λ is brain/blood partition coefficient. $fM_a(t)$ and $f\frac{M_b(t)}{\lambda}$ are the magnetization of water entering and leaving the brain, respectively. A well-mixed compartment is assumed. In a well-mixed compartment, these magnetizations are expected to be equal.

In the control experiment, no inversion pulse is applied in the presaturated slice, which means that $M_a(t)=M_0$ and $M(t=0)=0$. Therefore, the solution of Bloch equation is,

$$M_{ctrl}(t) = M_0(1 - e^{-\frac{t}{T_{1app}}}), \quad (2.5)$$

$$\frac{1}{T_{1app}} = \frac{1}{T_{1b}} + \frac{f}{\lambda}.$$

In tag experiment, inversion pulse is applied in the presaturated slice, which means that $M_a(t)=M_0(1 - 2\alpha e^{-\frac{t}{T_{1b}}})$ and $M(t=0)=0$. And, α is labeling efficiency defined as,

$$\alpha = \frac{M_0 - M_a(t=0)}{2M_0}. \quad (2.6)$$

Under above conditions, Bloch equation is solved. After that, the time dependent magnetization can be solved for as,

$$M_{tag}(t) = M_0(1 - 2e^{-\frac{t}{T_{1app}}}) - 2\alpha M_0 \frac{f}{\lambda} \frac{(e^{-\frac{t}{T_{1app}}} - e^{-\frac{t}{T_{1b}}})}{(\frac{1}{T_{1b}} - \frac{1}{T_{1app}})}. \quad (2.7)$$

The difference magnetization between control and tag experiment is then,

$$M(t) = M_{ctrl}(t) - M_{tag}(t) = 2\alpha M_0 \frac{f}{\lambda} \frac{(e^{-\frac{t}{T_{1app}}} - e^{-\frac{t}{T_{1b}}})}{(\frac{1}{T_{1b}} - \frac{1}{T_{1app}})}. \quad (2.8)$$

2.5.2 General Kinetic Model

Buxton formulated general kinetic model in order to quantify CBF in ASL-MRI. The general kinetic model directly derives from tracer kinetics theory. This theory is a mathematical description of the dynamic tissue concentration of any tracer delivered to the tissue by blood flow. In the general kinetic model, the tracer is considered as labeled blood water. So, labeled blood water is measured to quantity magnetization instead of the concentration. There are three functions for general kinetic model.

One of them is arterial input function which is called as the delivery of the tracer. The tagged blood acts as a radioactive agent. Therefore, half-life of tagged blood is stated as the longitudinal relaxation time of blood, T_{1b} . According to the single compartment model, $c(t)$, the normalized arterial concentration of magnetization arriving at time t in the brain, is modeled as,

$$c(t) = \begin{cases} 0, & 0 < t < \Delta t \\ e^{\frac{-t}{T_{1b}}} (\text{pulsed}), & \Delta t < t < \Delta t + \tau \\ e^{\frac{-\Delta t}{T_{1b}}} (\text{continuous}), & \Delta t < t < \Delta t + \tau \\ 0. & 0 < t < \Delta t \end{cases} \quad (2.9)$$

Delivery of the tracer is described as below,

$$AIF = (M_0 - M_b(t))c(t) = 2M_0\alpha c(t), \quad (2.10)$$

where, M_0 is magnetization under fully relaxed conditions, $M_b(t)$ is longitudinal magnetization per g of brain tissue, and α is labeling efficiency.

The other function is residue function, which is the fraction of tagged blood that arrived and is still in brain at time t . This function provides information about what happens to the tracer after arriving at the brain. Total amount of remaining tagged blood in brain slice is described as,

$$q(t) = q_0 - q_0 H(t), \quad (2.11)$$

where, q_0 is the quantity of labeled blood in the beginning, and $q_0H(t)$ is the total amount of tracer leaving the brain slice. Therefore, residue function is described as,

$$r(t) = 1 - H(t) = \frac{q(t)}{q(0)} = e^{-\frac{ft}{\lambda}}, \quad (2.12)$$

where, f is blood flow and λ is brain/blood partition coefficient. [19]

The last function is the relaxation function, which is the fraction of the original longitudinal magnetization of tagged protons carried by blood, denoted as,

$$m(t) = e^{-\frac{t}{T_{1t}}}, \quad (2.13)$$

where, T_{1t} is the longitudinal magnetization of the tissue. So, Buxton describes time dependent tissue signal as [4],

$$c(t) = f \int_0^t AIF(\tau)r(t-\tau)m(t-\tau)d\tau. \quad (2.14)$$

As a result, $\Delta M(t)$ can be modeled as,

$$\Delta M(t) = \begin{cases} 0, & 0 < t < \Delta t \\ 2M_0f(t-\Delta t)\alpha e^{-\frac{t}{T_{1b}}}q_p(t)(pulsed), & \Delta t < t < \Delta t + \tau \\ 2M_0f(t-\Delta t)\alpha e^{-\frac{\Delta t}{T_{1b}}}q_p(t)(continuous), & \Delta t < t < \Delta t + \tau \\ 2M_0f\tau\alpha e^{-\frac{t}{T_{1b}}}q_p(t)(pulsed), & \Delta t + \tau < t \\ 2M_0f\tau\alpha e^{-\frac{\Delta t}{T_{1b}}}q_p(t)(continuous), & \Delta t + \tau < t \end{cases} \quad (2.15)$$

and,

$$\begin{aligned} q_p(t) &= \frac{e^{kt}(e^{-k\Delta t} - e^{-kt})}{k(t-\Delta t)}, & \Delta t < \Delta t + \tau \\ q_p(t) &= \frac{e^{kt}(e^{-k\Delta t} - e^{-kt})}{k(t-\Delta t)}, & \Delta t < \Delta t + \tau \\ k &= \frac{1}{T_{1b}} - \frac{1}{T_1'}, \\ \frac{1}{T_1'} &= \frac{1}{T_{1t}} + \frac{f}{\lambda}. \end{aligned} \quad (2.16)$$

In addition to this, Chappell et al. [34] proposed that the difference of control and label images included intravascular (IV) and extravascular (EV) components. IV

component represents that some of labeled blood remains in vessels, whereas EV component represents that some of the labeled blood remains in tissue. This is important to keep in mind to correct CBF maps and include IV component. And, the total signal, which is the difference of control and label images, is the sum of these two components as,

$$\Delta M = \Delta M^{(tissue)} + \Delta M^{(aBV)}. \quad (2.17)$$

IV component, $\Delta M(t)$, is modeled as,

$$\Delta M^{(abv)}(t) = \begin{cases} 0, & t < \Delta ta \\ 2M_{0b}\alpha e^{\frac{-t}{T_{1b}}} aBV, & \Delta ta < t < \Delta ta + \tau a \\ 0, & \Delta ta + \tau a < t \end{cases} \quad (2.18)$$

where, aBV represents the arterial blood volume fraction, Δta is the bolus arrival time (BAT), and τa is the bolus duration (seconds) of the arterial bolus.

2.5.2.1 QUIPSS II

An inversion pulse is applied in tag slice in this technique. After some time, tagged blood arrives into the imaging slice. If images are acquired before tagged blood flows into the imaging slice, it causes errors in the estimation of CBF maps, which is a problem. Multiple phases overcome this problem. ASL-MRI experiment is applied at multiple phases. This solution can increase the accuracy of perfusion measurements. However, this causes long data acquisition time reducing signal-to-noise (SNR). Therefore, this protocol is sensitive to motion artifacts. The most popular pulsed ASL technique is quantitative imaging of perfusion using a single subtraction (QUIPSS and QUIPSS II) [5], which uses additional pulses to saturate the trailing edges of the label, thus producing a clearly defined bolus. The OUIPSS labeling scheme is implemented in order to eliminate these variable transit delays. This technique is based on a multi-TI PASL sequence. In this technique, saturation pulses are applied. A saturation pulse is applied to the imaging slice at time TI1 after the arterial blood is tagged. After some

time, the image is acquired. In QUIPPS, the saturation pulse is applied in imaging slice. Unlike QUIPSS, the saturation pulse is applied to the tagging region in QUIPSS II. QUIPSS II provides more time for the distribution of tagged arterial blood, which has arrived to the tissue, with respect to QUIPSS. Furthermore, it produces homogeneous and more robust perfusion signal. In QUIPSS II, CBF (f) is calculated using the difference of control and tag images acquired at multiple times by means of the following formula [5],

$$\Delta M = 2M_{0b}fTI_1e^{\frac{-TI_2}{T_{1b}}}q(T_{1b}, T_{1t}, T_{ex}, f, \lambda, TI_2), \quad (2.19)$$

for

$$\begin{aligned} TI_1 &< \tau, \\ TI_2 &> TI_1 + \delta t. \end{aligned} \quad (2.20)$$

where, M_{0b} is fully relaxed magnetization of blood, T_{1b} is the longitudinal relaxation time of arterial blood, T_{1t} is the longitudinal relaxation time of arterial blood within tissue, T_{ex} is exchange time, TI_2 is the time of acquisition image, λ is the blood partition coefficient of water, τ is the time width of the tag, and δt is the transit time of blood from the tagging region to the imaging slice. q is a correction factor for the difference in relaxation time of tissue and is close to unity [17].

2.5.2.2 QUASAR

Quantitative Star Labeling of Arterial Region (QUASAR) was proposed by Petersen et al. aiming at providing more accurate quantification of brain tissue perfusion [6]. In this technique, CBF maps were quantified by modifying general kinetic model with Look-Locker readout and QUIPSS II.

During evolution of QUASAR, first Pulsed Star Labeling of Arterial Regions (PULSAR) was introduced by Golay et al. [35]. PULSAR is based on the original EPISTAR sequence. This means that PULSAR is a STAR labeling technique coupled with a 2D multi-slice EPI readout. In this technique, water suppression pulse is used in

order to presaturate the imaging slice, which increases the sensitivity of the perfusion signal. Before development of PULSAR, there was regional perfusion imaging technique (RPI), which had serious drawbacks. It provided regional CBF measurement of individual feeding arteries. However, this technique is very susceptible to magnetic field inhomogeneities. Therefore, it isn't practical for high field imaging. PULSAR is developed to overcome these limitations. With respect to RPI method, the PULSAR technique is less sensitive to field inhomogeneities. Moreover, this technique has better labeling efficiency and higher SNR.

QUASAR is the combination of PULSAR with QUIPSS II and Look-Locker readout. This technique is preferred to sample at multiple time points of perfusion signal, which makes a clear definition of the arterial blood bolus. In this technique, both labeling and control experiments are preceded by a saturation pulse and QUIPSS II type of bolus saturation is applied during a Look-Locker sampling [32]. Moreover, a vascular crusher is applied at certain intervals. As a result of performing ASL with and without the application of a vascular crusher, crushed and non-crushed control-label pairs are acquired for the estimation of AIF and arterial blood volume (aBV). When the vascular crusher is applied, CBF of the micro-vascular compartment (CBF_{crushed}) is measured. On the contrary, a CBF of the macro- and micro-vascular compartments together (CBF_{non-crushed}) is measured in the absence of a vascular crusher. Arterial transit time (ATT) is defined by the ratio of the perfusion signal of CBF_{non-crushed} to CBF_{crushed}, which is defined as the time it takes for the labeled blood to travel from the labeling plane to the micro-vascular compartment of the imaging voxel [6].

Figure 2.8 shows the overall sequence of QUASAR. In Figure 2.8.a, labeling and control experiments are followed by the multi-time point in the course of τb , which is the temporal length of the labeled blous obtained with a bolus saturation technique similar to QUIPSS. For the duration of τs (shown in gray), a multislice readout is implemented. Figure 2.8.b and c show the sequence of the noncrushed and crushed experiments, respectively. These experiments are done by applying bipolar gradients in order to suppress intravascular signal. These gradients have the same magnitude but opposite direction. In Figure 2.8.d, the actual RF and gradient scheme for pre-

saturation, label/control, postsaturation, bolus saturation, and excitation followed by readout with or without crusher is given. The readout techniques are same for non-vascular crusher and vascular crusher. Figure 2.8.e shows pulses applied in the control experiment. Because this technique is based on EPISTAR, two 180° RF pulses are applied in the control experiment. In figure 2.8.f, the images located from left to right represent presaturation slab, label/control region, post saturation slab, image acquisition without bolus saturation, and image acquisition with bolus saturation, respectively [6].

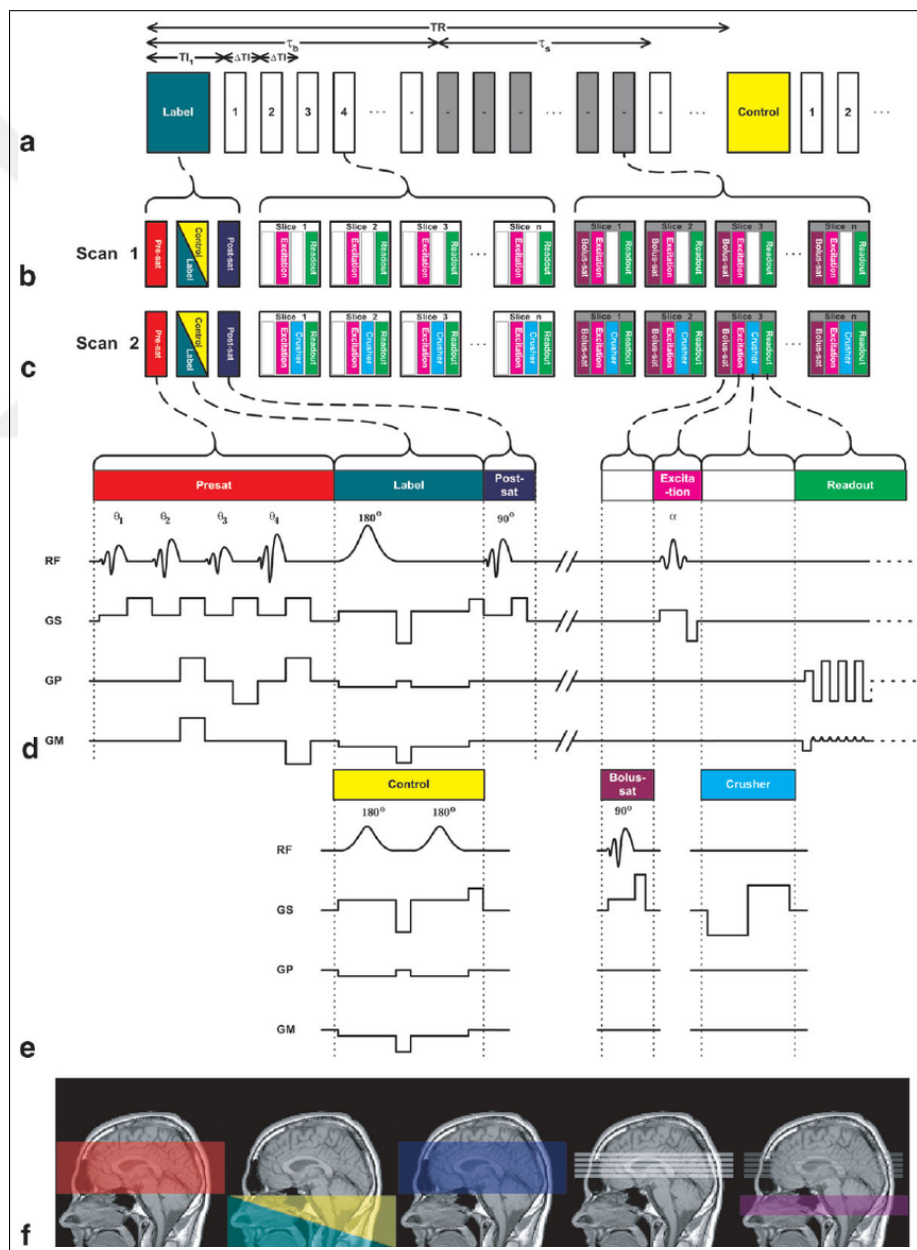


Figure 2.8 A QUASAR sequence diagram [6].

There are two different magnetizations coming from CBFnon-crushed and CBF-crushed. Therefore, total magnetization is the sum of these two magnetizations. ΔM is formulated as,

$$\Delta M = \Delta M^{crushed} + \Delta M^{non-crushed}. \quad (2.21)$$

The main assumption is that the subtraction of control and label signals is ideally perfect. As a result of this, ΔM (non-crushed) can usually be ignored. Thus, the measured signal doesn't include subtraction errors. Briefly, total signal depends only on the difference of the control and label signals, and this difference gives a direct measure of how much blood has been delivered to the voxel and survived at the time of measurement [6].

AIF can be obtained by subtracting the difference signal of the noncrushed data from the difference signal of the crushed data. aBV is obtained as the time integral of the arterial signal curve divided by the bolus area that corresponds to an initially labeled voxel with 100% blood volume. aBV can be expressed as,

$$aBV = \frac{\int_{-\infty}^{+\infty} (\Delta M_{ncr}(t) - \Delta M_{cr}(t)) e^{\frac{t}{T_{1b}}} dt}{2M_{a0}\tau\alpha}. \quad (2.22)$$

2.6 Literature Review

There have been a few studies measuring CBF in PD-MCI patients using ASL-MRI. The general target of these studies has been defining biomarkers identifying PD-MCI in the early stages of PD. The diagnosis of PD-MCI is important, because patients with PD-MCI are at increased risk of developing dementia later. Anticipated biomarkers may help in identifying patients that might have dementia later in life, and these patients might be provided with possible therapies that might slow down the progression of dementia. Decreased perfusion in parieto-occipital cortex, cuneus, precuneus and posterior cingulate gyrus in PD compared to healthy controls (HC)

has been reported in the literature [7]. The limitation of that study was using four Tis, and the whole brain wasn't scanned. In another study, Chao et al. [9] observed reduced perfusion in the right precuneus, right inferior parietal cortex, right middle cingulum, and right middle frontal cortex in MCI subjects, who later became demented, in comparison to MCI subjects who remained nondemented. Another study reported decreased perfusion in the inferior and middle temporal gyri, fusiform gyrus, inferior and superior lateral occipital cortex, supracalcarine and intracalcarine cortex, cuneus, precuneus, posterior cingulate gyrus, superior parietal lobule, and right middle frontal gyrus in PDD versus HC [8]. These studies all used a single TI. In the literature, it has been reported that multi TI is more effective in calculating CBF maps than single TI [10].

3. MATERIALS and METHODS

3.1 Subjects

19 PD-MCI patients and 19 cognitively PD-CN patients were included in this study. PD-MCI were matched to PD-CN for age, sex ratio and years of education. The age of participants ranged from 40 to 80 years. All subjects provided written informed consent after the nature of the examination was explained. The study protocol was approved by Istanbul University Clinical Research Ethics Committee. Table 3.1. shows the age range, sex and education level of all patients.

Table 3.1
Demographics of patients.

Variables		PD-MCI	PD-CN
Sex	Male	12	15
	Female	7	4
Age Groups	40-50	2	3
	50-60	7	9
	60-70	7	4
	70-80	3	2
Education	5-8	11	7
	8-11	1	2
	11-15	7	10

3.2 Diagnostic Criteria and Assessment

All subjects were examined by expert neurologists. There were specific and common criteria for the selection of the subjects. One important criterion for determining subjects was the years of education to carry out the clinical tests successfully. Therefore, at least a certificate of primary education was needed from all subjects. Afterwards, the subjects were asked whether they have received any antidepressant treat-

ment, because antidepressants have been reported to affect the regional blood flow in the brain [36]. If a subject has taken any antidepressant pill, she/he weren't included in the study. In the final step, Geriatric Depression Scale (GDS) was performed to assess depression, since depressed patients could have alterations of CBF with respect to non-depressed people [37]. Then, the severity of disease and the general neuropsychological status of the selected subjects were assessed to form their Unified Parkinson's Disease Rating Scale (UPDRS).

UPDRS is a test that can be used to quantify motor manifestations of PD. The UPDRS applied in this study consisted of four subsections. Subsection 1 included mental, behavioral, and mood questions. In subsection 2, questions related to activities of daily living were asked. Subsection 3 was a clinician's rating of the motor manifestations of PD. Subsection 4 rated complications of therapy. Results obtained from these subsections were evaluated by the interviewer and clinical observation. Subsections 1, 2, and 4 consisted of information received from patients or caregivers, whereas data for subsection 3 was based on examination of patient's motor symptoms. The total score of UPDRS provides insight into a patient's disease progression [38].

3.2.1 Assessment of Cognitive Impairment

Neurophysiological tests were performed for all the subjects. These tests provided information about cognitive status of the subjects. Also, these tests were used for assessing the degree of PD. The combination of results of UPDRS and these tests were conducive to determine whether a patient with PD is mild cognitively impaired or cognitively normal. The following tests were performed in this study.

3.2.1.1 Stroop Test

In 1935, the Stroop effect was described by John Ridley Stroop. The Stroop effect, sometimes called the Stroop test, measures attention. In this test, a sheet where

names of colors appeared in congruent or incongruent ink is shown to participants. Stroop effect consists of two parts. The first test is easy, since the color and the word are same. However, second part is difficult with respect to the other, because the color and meaning of the word are incongruent. And, participants want to read words, which is another color's name. Reading is faster than naming the colors, which creates a conflict in brain. Finishing the test requires a long time because the brain has to suppress the wrong answer [39].

3.2.1.2 The Wisconsin Card Sorting Test

The Wisconsin Card Sorting Test (WCST) ensures a versatile measure of neuropsychological functioning to clinicians. The use of WCST has become widespread as a clinical neuropsychological instrument. It assesses abstract thinking, cognitive flexibility, and impairment. In this test, stimulus cards with shapes on them are shown to the participants. The cards have different colors, numbers, and forms of shapes. Firstly, participant is supposed to sort these cards into two piles. What stimulus dimension is used in order to sort the cards isn't told to the participant. However, if the match is accurate, this is told to the participant [40].

3.2.1.3 The Benton Judgment of Line Orientation Test

The Benton Judgment of Line Orientation Test has been increasingly employed as a measure of spatial perception in both clinical and research settings. In this test, there are line segments of different spatial orientations, which must be matched with a set of longer lines on a response card. In order to complete the test, a participant must match correctly a set of five practice items. Total score is based on the number of correct items adjusted with age and gender. Scores categorizes the participants as normal, mild, moderate, and severely impaired [41].

3.2.1.4 The Symbol Digit Modalities Test

The Symbol Digit Modalities Test (SDMT) was developed in order to determine participants with neurological impairment. The SDMT examines neurocognitive functions including attention, visual scanning, and motor speed. Also, it is easy to administer. In this test, the task sequence includes a series of symbols, each with a blank space underneath. Within a 90-second time limit, participant is supposed to insert the numbers associated with the symbols. The test can be administered in both written and oral forms [42].

3.2.1.5 The Addenbrooke's Cognitive Examination Revised

The Addenbrooke's Cognitive Examination Revised (ACER) is employed to identify mild cognitive impairment and dementia in both clinical and research settings. This test measures five cognitive domains including attention/orientation, memory, verbal fluency, language and visuospatial abilities. There are questions related to these domains. Total score of ACER is 100. High scores show better cognitive functioning [43].

3.3 Data Acquisition

All subjects were scanned using 3 Tesla clinical MR system (Philips Medical Systems, Achieva, Holland) with a 32-channel head coil at Hulusi Behcet Life Research Center in Istanbul University. In this study, a T2-weighted (T2w) MR image was acquired for each patient (TR/TE 10243/80 *ms*, flip angle 90°, FOV 240x240 *mm*², slice thickness=2 *mm*, matrix size =128x128, total scan duration=210 *sec*). Figure 3.1 shows an example of an axial T2w MR image in a subject with PD-CN.

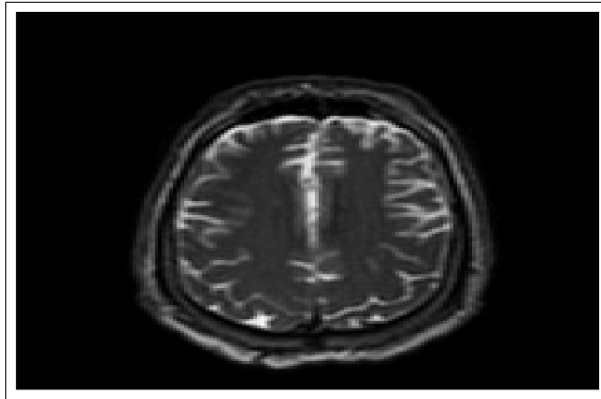


Figure 3.1 T2-weighted MR image.

ASL-MR images were acquired by using STAR labeling with multi-slice single-shot EPI readout at multiple TI. Figure 3.2 shows the ASL-MRI sequence which is used in Philips Achieva 3T scanners. Bipolar gradients and background suppression were not applied. The sequence employs QUIPSS II technique that applies presaturation pulses in the volume of interest at multiple times. Afterwards, a 90° dephasing pulse is applied within the same region of the presaturation pulses to provide a clear starting time of the bolus. Also, there are wet saturation pulses used in order to suppress water like in spectroscopy technique [35]. ASL-MR imaging parameters were as follows; TR/TE=250 ms/16 ms, flip angle=40°, FOV 240x240 mm²; matrix size=80x80, 6 slices, slice thickness=6 mm, multi-slice single-shot EPI; SENSE 1.2, label thickness=130 mm, label gap=20 mm, label delay 300 ms, number of dynamics=48, total scan duration=248 sec. At a single ASL-MRI scanning session, 6 slices were acquired at a certain region of brain. Each slice was acquired at 8 different phases using 8 distinct TI that are 250 ms apart. Figure 3.3 shows an example of the 6 slices acquired at eight different TI's. For the first slice, minimum TI was 300 ms, and the maximum TI was 2050 ms. The minimum TI of each consecutive slice was increased by 25 ms of that of the previous slice. Also, data acquisition was repeated 30 times at each phase and slice in order to increase SNR. The ASL-MRI data acquisition was repeated three times to cover the whole brain.

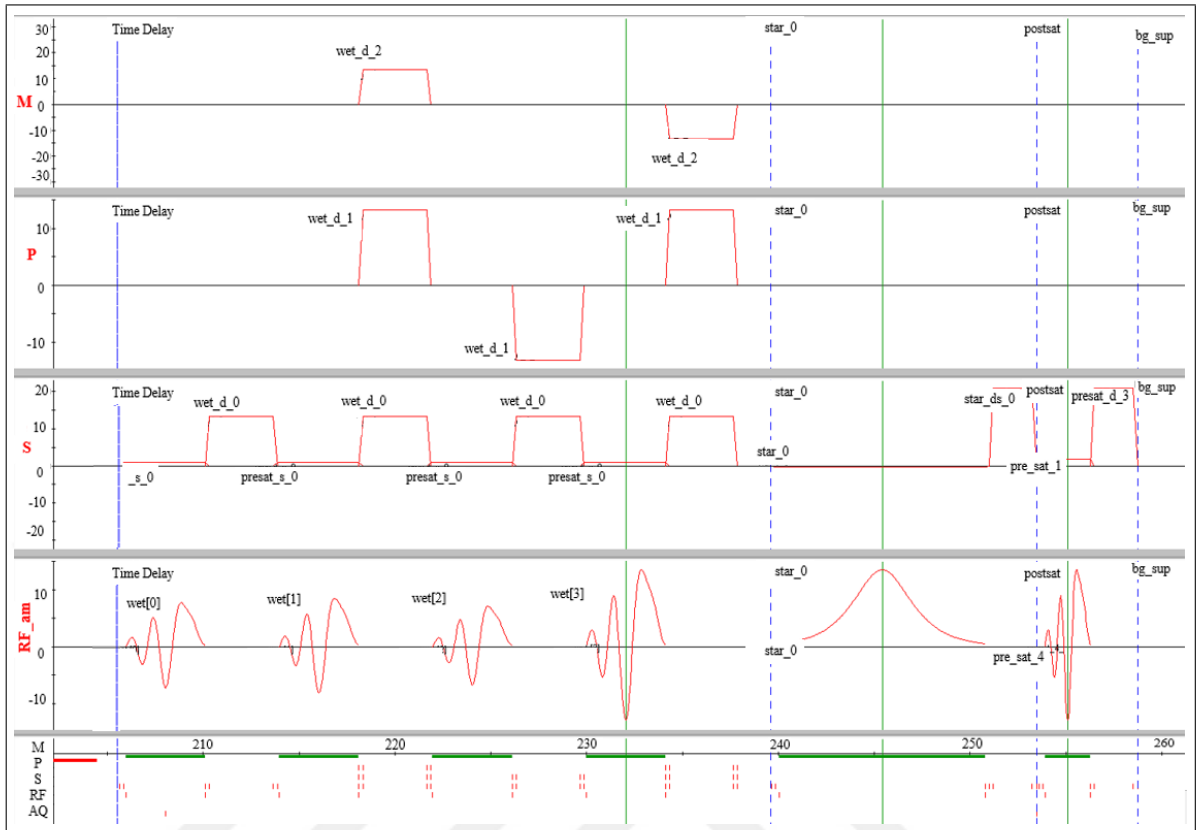


Figure 3.2 Pulse sequence diagram of ASL-MRI in Philips Achieva 3T scanners.

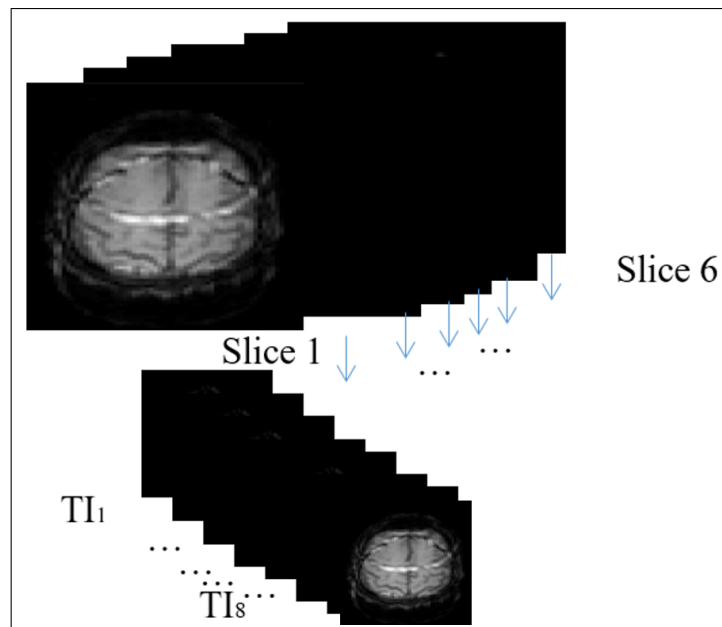


Figure 3.3 The demonstration of slices at different TIs.

3.4 Data Processing and Analysis

3.4.1 CBF and aBV Map Calculation

After scanning the subjects, 1440 control and 1440 tag images were obtained by applying STAR labeling with EPI readout at multi times. A program was written in MATLAB(The Mathworks Inc., Natick, MA) for calculating the CBF and aBV maps. In the first step, the images were arranged according to their slice locations. After that, control and tag images were averaged and deltaM images were obtained by subtracting average control images from tag images, respectively. In Figure 3.4, one control image subtracts from one tag image in order to get one deltaM image.

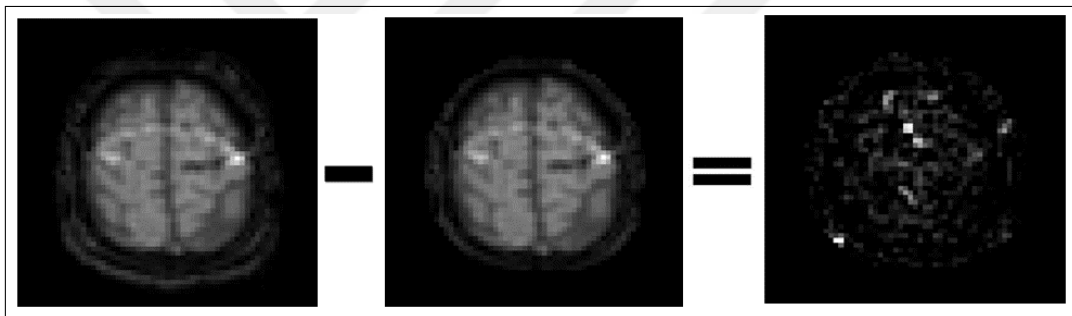


Figure 3.4 The subtraction of control and tag images.

Before CBF calculation, brain tissue was masked at each session to remove out-of-brain voxels in average control and deltaM images. In Figure 3.5, masking of a single control image is shown. The main magnetization, M_0 , was estimated for each pixel of

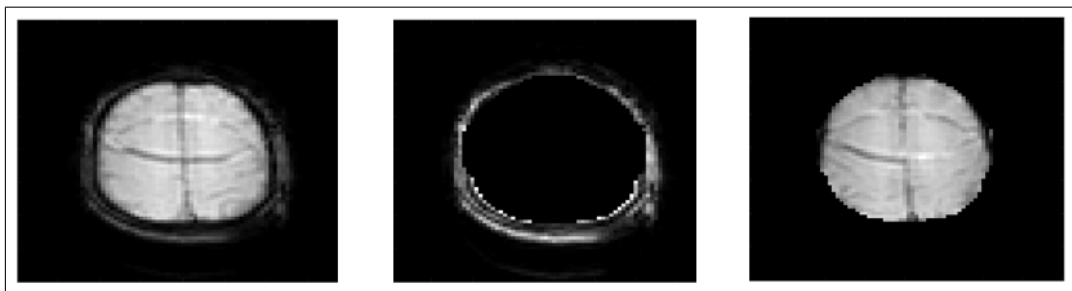


Figure 3.5 Masking in a control image. a) Control image at a given slice, b) masked out tissue, and c) masked control image of the slice.

control images using different phases of the control images by employing the following formula,

$$M(TI) = M_0(1 - e^{-\frac{TI}{T_{1b}}}), \quad (3.1)$$

where TI is the inversion time, T_{1b} represents the longitudinal relaxation of blood. M_0 correction was used in CBF calculation. Additionally, the effect of using a constant M_0 in CBF calculation was explored. In the second step, CBF maps was calculated for each patient by taking into consideration aBV correction using QUIPSS II formula based on General Kinetic Model [4, 5, 34] that was described in detail in the Background section.

3.4.2 Registration to MNI152 Brain Atlas

ASL images were registered to structural images, which were T2w MR images in this study. Forty-eight CBF maps and ninety T2w MR images of each subject were converted to .nii format in Mricron program (<https://www.nitrc.org/projects/mricron>). The skull of each T2w MR image was stripped in FMRIB Software Library (FSL) (<http://fsl.fmrib.ox.ac.uk/fsl/fslwiki/>) software package [44]. Figure 3.6 shows the T2w MR image of a PD-CN patient after skull removal.

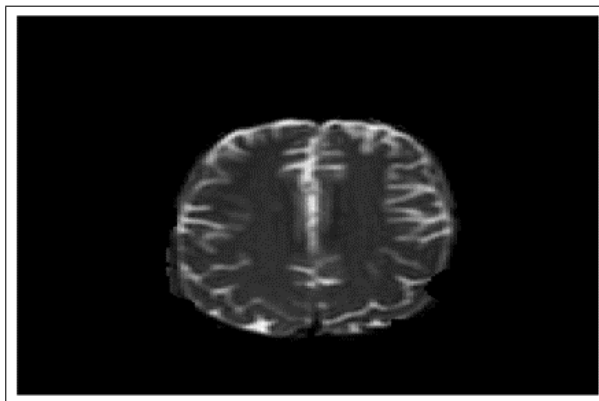


Figure 3.6 T2w MR image of a subject after removing skull.

CBF maps were resampled into T2w MR image spatial resolution. Then, T2w

MR image intensities were replaced with CBF map intensities at corresponding slice locations using a program written in MATLAB. Figure 3.7 shows an example brain after CBF maps were correctly fused into T2w MR images. In two patients, CBF-T2w MR image fusion failed due to subject motion, and an example of failure is shown in Figure 3.8.

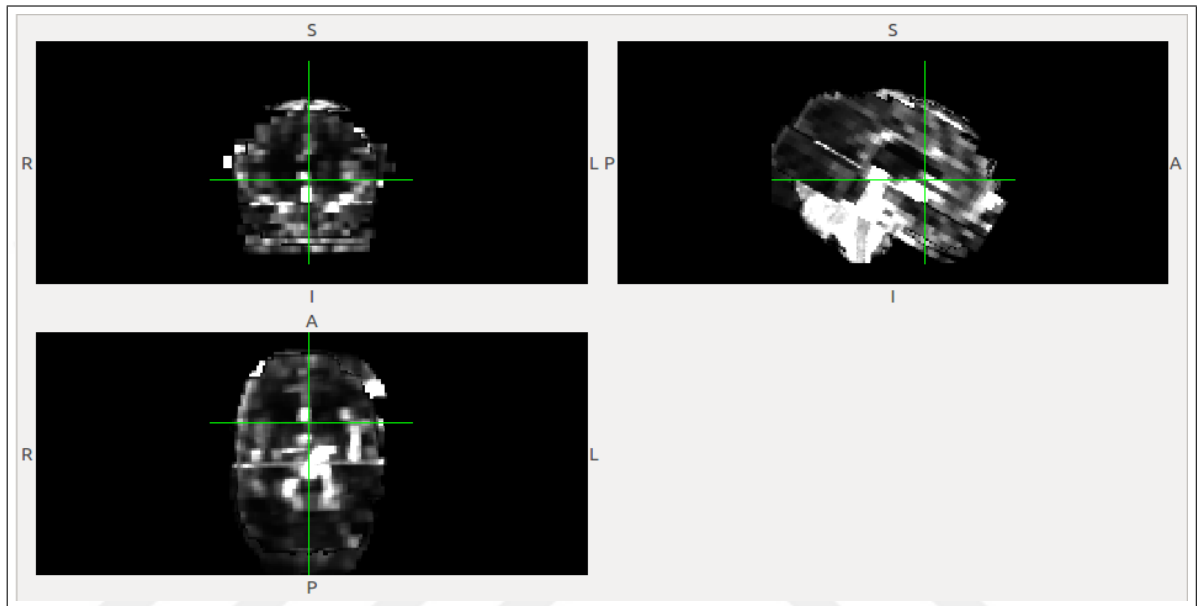


Figure 3.7 The FSL view of CBF-T2w MR fused image.

Afterwards, the CBF-T2w MR fused images were resampled into the MNI152 atlas. Figure 3.9 shows the MNI152 atlas in FSL. Then, CBF values of several brain regions were estimated in FSL using MNI152 registered CBF maps.

3.4.3 Histogram Analysis

A histogram analysis was applied to assess the change in CBF maps after aBV correction. The histogram of one slice of the CBF map calculated with or without aBV correction, which had high arterial signal, acquired from a PD-CN patient was selected and histograms were evaluated using an in-house program written in MATLAB. The histogram analysis provides a general idea of the data shape. In our study, the skewness, kurtosis, peak height and peak position of histograms were evaluated. The skewness

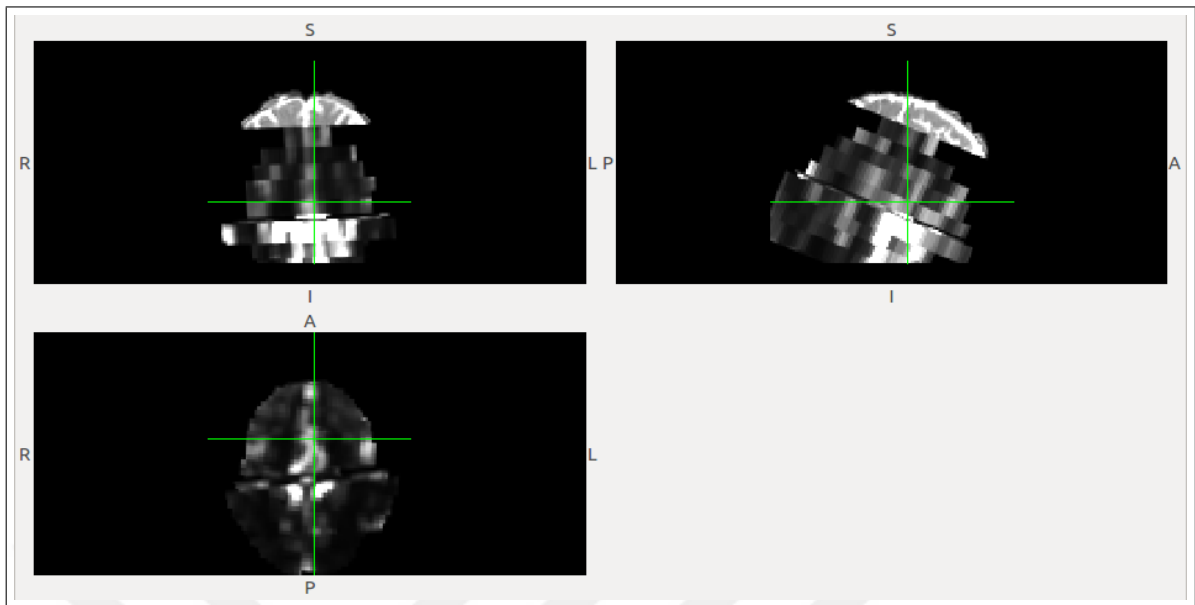


Figure 3.8 The FSL view of a CBF-T2w MR incorrectly fused image due to subject motion.

indicates whether a data set is symmetric or skewed to one side. If data set is perfectly symmetrical, skewness is equal to zero, which means that histogram looks the same to the left and right of the center point. A positive value for skewness means that distribution is skewed towards the right, whereas a negative value means that the distribution is skewed towards the left. Kurtosis provides information about the central peak of the data set. Higher values in kurtosis demonstrate a higher, sharper peak in data, while lower values in kurtosis demonstrate a lower, less distinct peak. The skewness and kurtosis have no units. In addition to skewness and kurtosis, peak height and peak positions were calculated. The peak height shows the value of highest peak in the data. The peak position gives the location of the peak [45].

3.4.4 Graphical User Interface Design

In this study, a graphical user interface (GUI) was designed in MATLAB for CBF map calculation. The control, tag and deltaM images were shown in different axes after ASL-MRI images were selected. The M_0 fit in a selected pixel was displayed

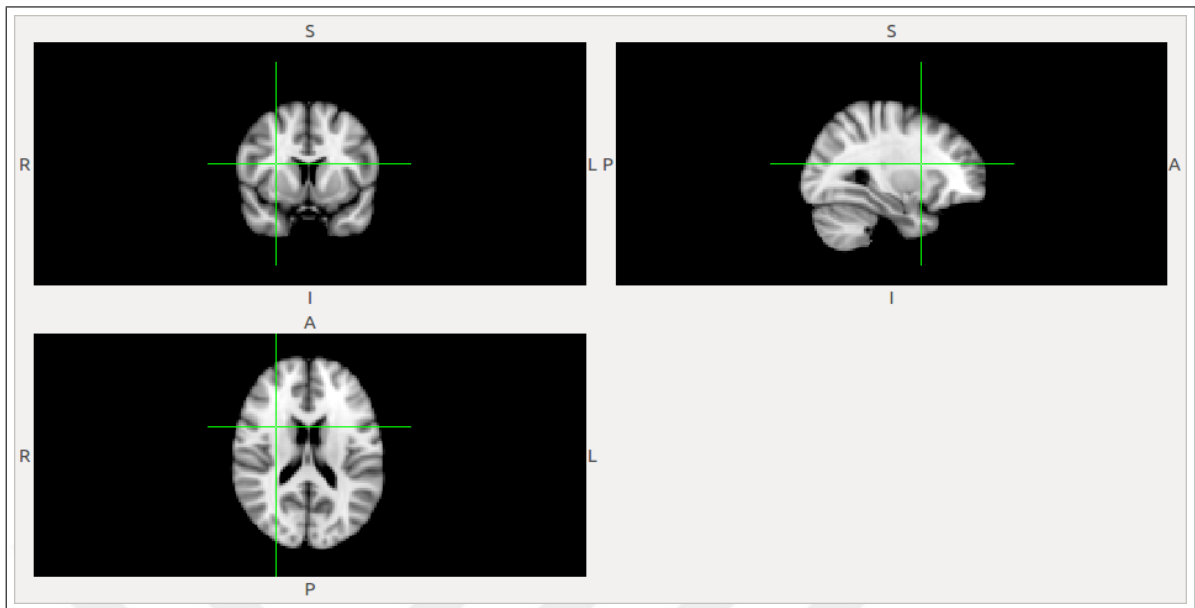


Figure 3.9 The FSL view of MNI152 atlas.

in another frame. The second step was the calculation of CBF maps. The option of running CBF calculation with QUIPSS II and Look-locker techniques were provided in different drop down menu options. After selecting the processing technique, CBF and aBV maps and CBF fit function in a given pixel were shown in different axes. Although these CBF calculations are all based on general kinetic model, different formulas have been applied for calculating CBF maps. In this study, there were not any bipolar gradients and background suppression for ASL-MRI data acquisition. Besides, there were pre- and post- saturation pulses applied in the region of interest at multiple times. Therefore, QUIPSS II technique was selected for CBF processing. The design of the graphical user interface is shown in Figure 3.10. This GUI enabled a more convenient CBF estimation in MATLAB.

3.4.5 Statistical Analysis

The ASL-MR images were acquired from two independent groups, including PD-MCI and PD-CN. A Mann-Whitney ranksum test was used to understand whether there was a statistically significant difference between the mean CBF values in several

brain regions of PD-MCI and PD-CN. A Wilcoxon signed rank test was applied to compare histogram parameters of the CBF maps before and after aBV correction. Bonferroni multiple comparison correction was used for adjusting p values for the statistical analysis. Additionally, Spearman correlation coefficients were calculated to assess if there was a relationship between neuropsychological test scores and CBF values. Moreover, Friedman test with SNK test for multiple comparisons was used to compare the CBF values in different brain regions of each group.



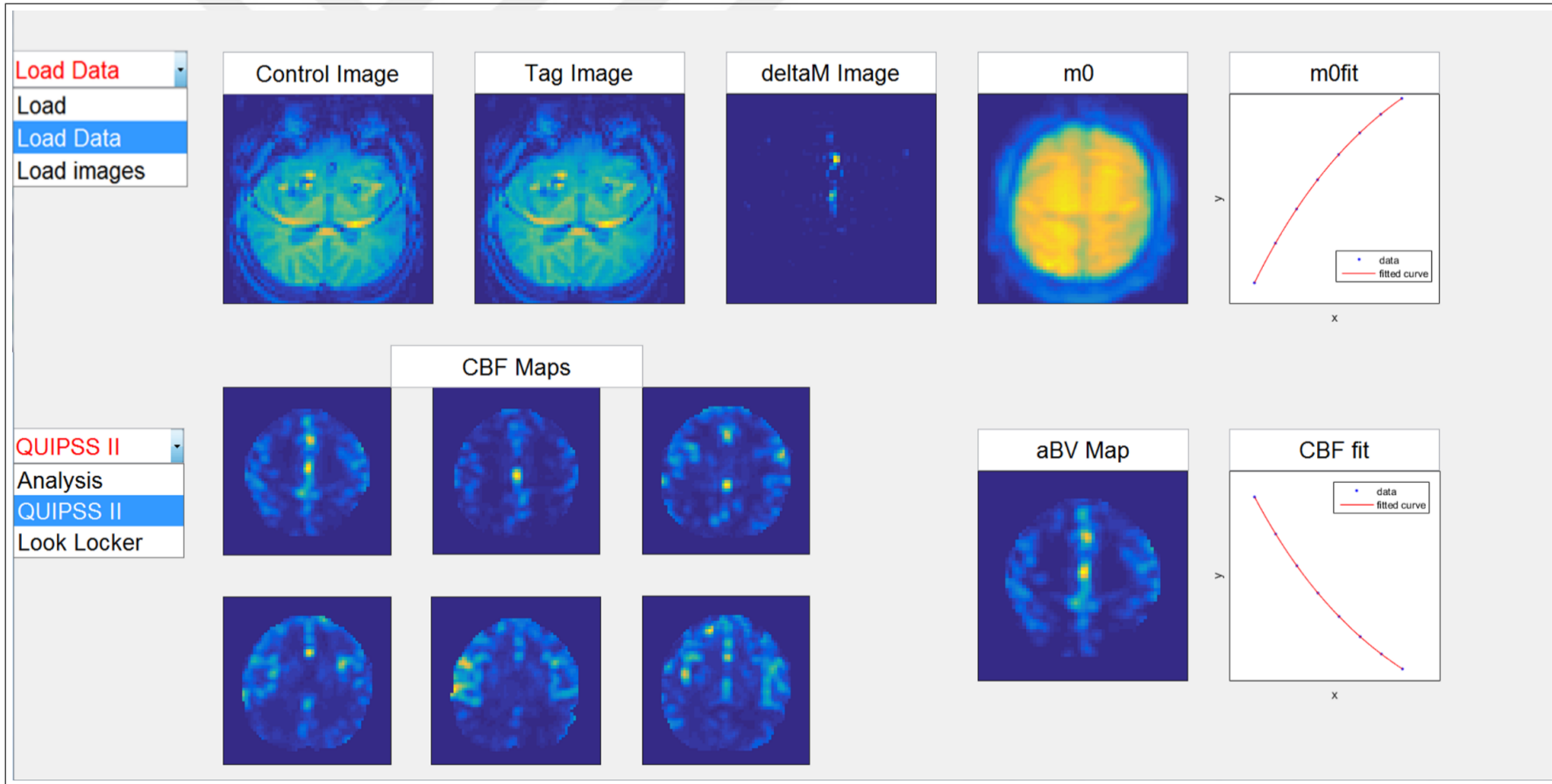


Figure 3.10 The GUI of CBF map calculation.

4. RESULTS

4.1 The CBF and aBV Values

CBF and M_0 were calculated and their maps were generated. Figures 4.1, 4.2 and 4.3 show the estimated M_0 maps estimated in three distinct regions of a PD-CN patient. Figure 4.4 shows the M_0 fitting in a single pixel. The range of M_0 was [0 40000].

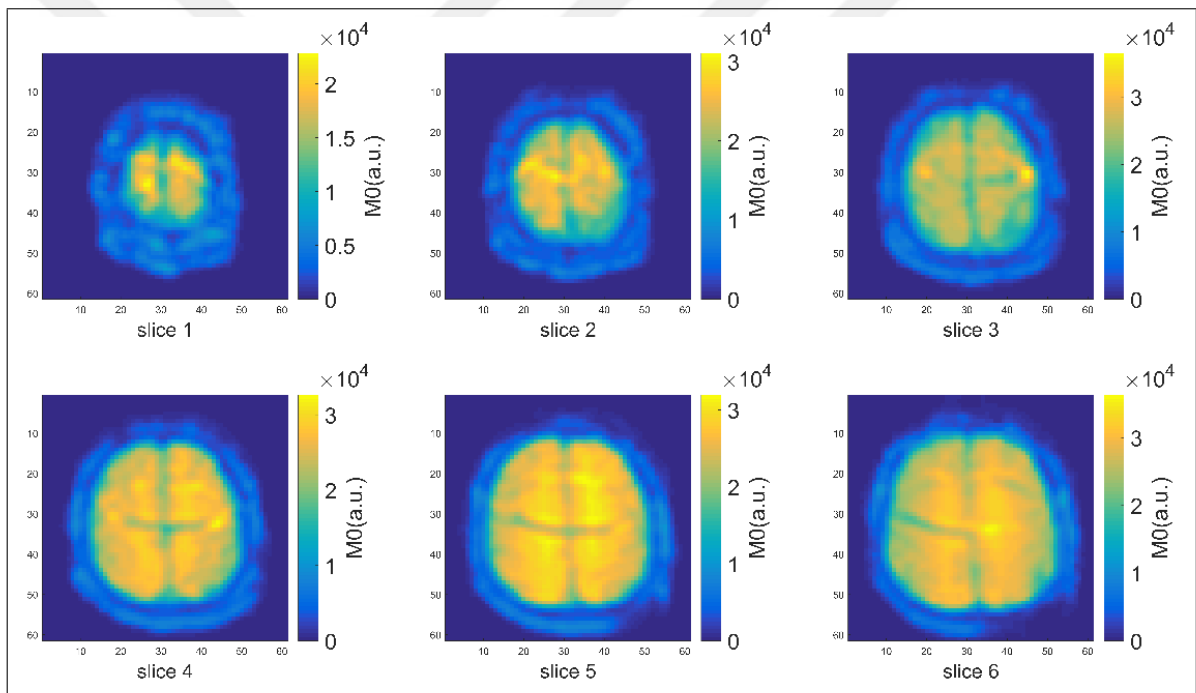


Figure 4.1 M_0 maps taken from 1st region of a PD-CN patient.

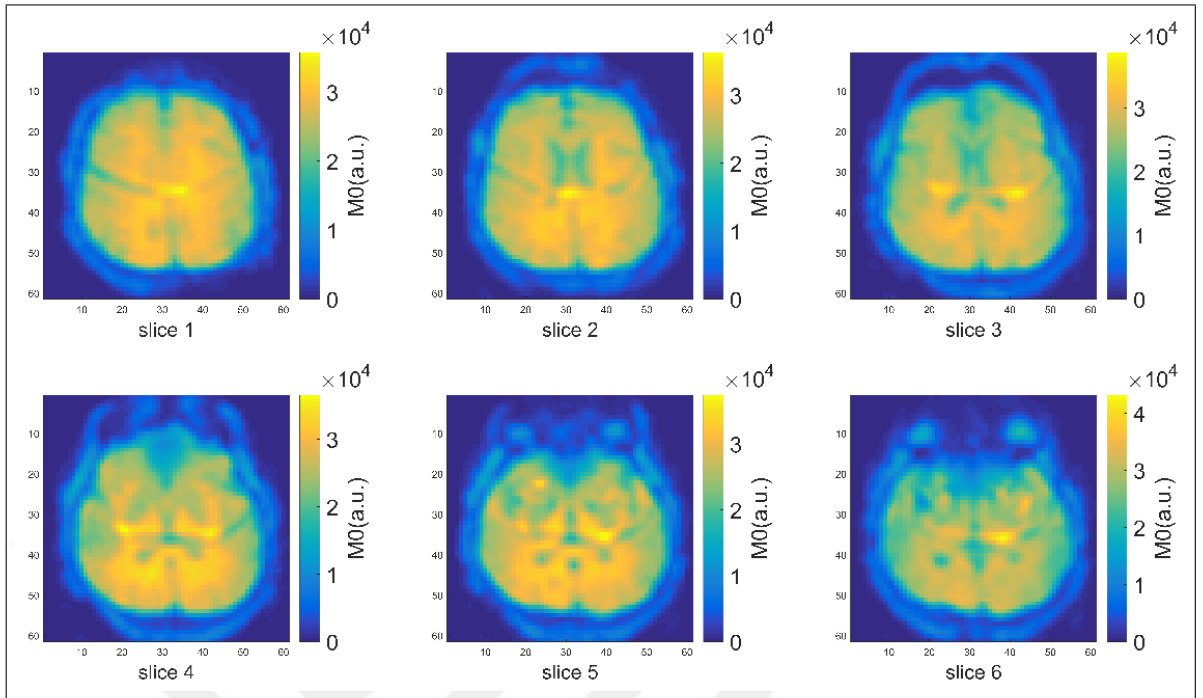


Figure 4.2 M_0 maps taken from the 2nd region of a PD-CN patient.

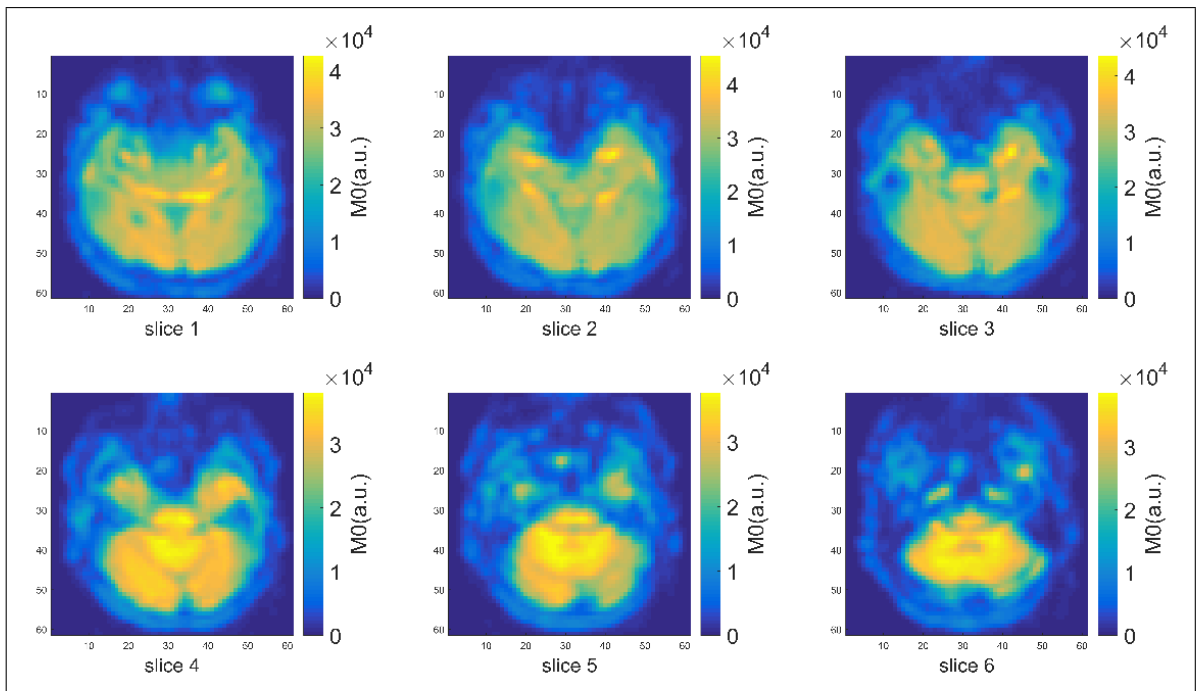


Figure 4.3 M_0 maps taken from the 3rd region of a PD-CN patient.

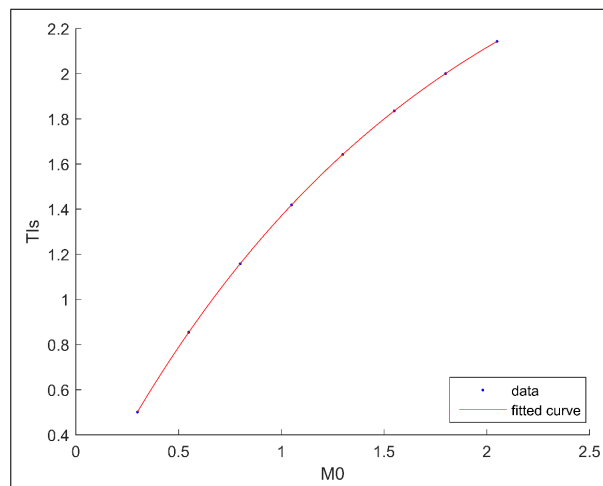


Figure 4.4 M_0 fit in a given pixel.

Figure 4.5 shows the CBF map estimated with a constant M_0 , which was taken as 1000. When the value of M_0 was accepted as a constant without calculating its real value, the range of CBF was [0 2500], even though the expected CBF value range is [0 80]. In Figure 4.6, the CBF map estimated with calculated M_0 is shown, which had an expected range of [0-80].

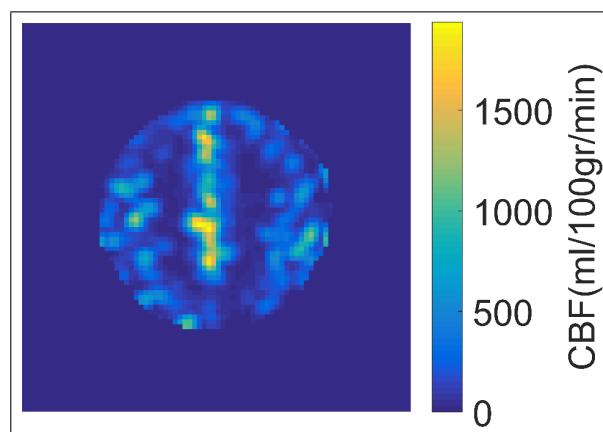


Figure 4.5 The CBF map calculated with a constant M_0 .

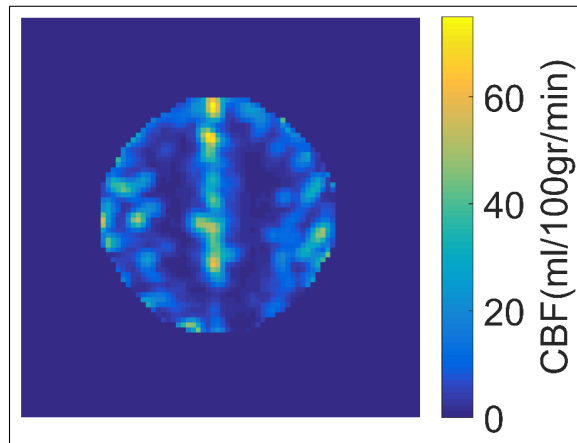


Figure 4.6 The CBF map calculated with real M_0 values.

Figures 4.7, 4.8 and 4.9 show the CBF maps in three distinct regions of the brain. The ranges of CBF maps were $[0\ 80]$, $[0\ 150]$ and $[0\ 600]$ in these regions, respectively. Figure 4.10 shows aBV maps taken from the first region of a PD-CN patient. The range of aBV maps in this region was $[0\ 1]$.

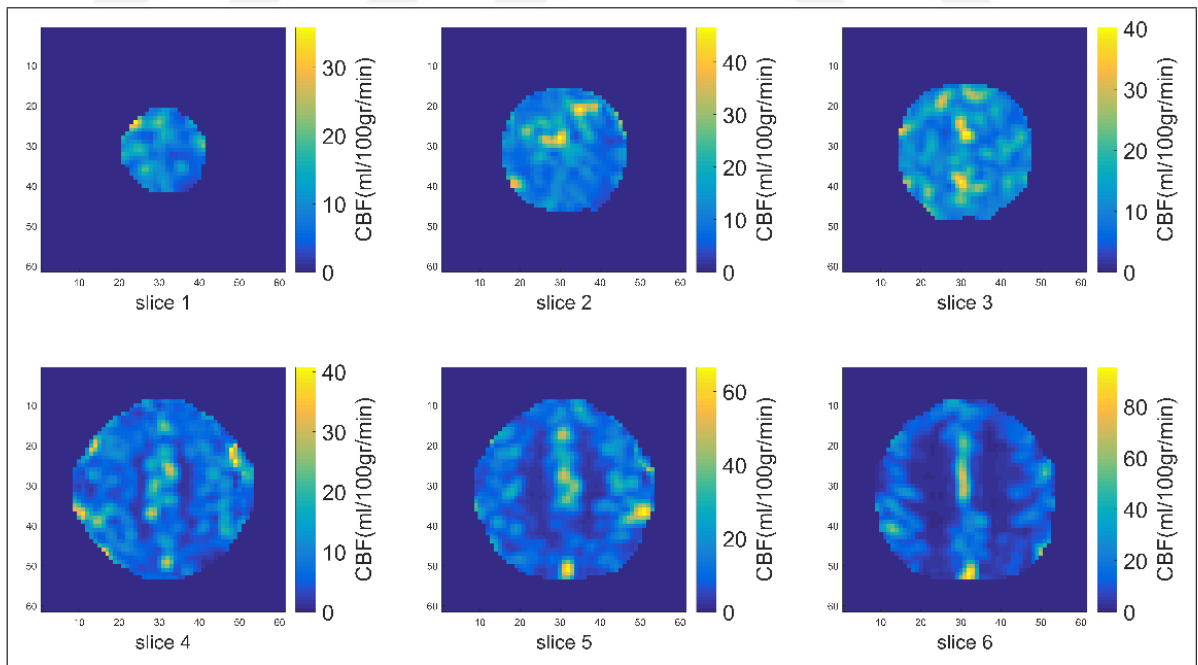


Figure 4.7 CBF maps taken from the 1st region of a PD-CN patient.

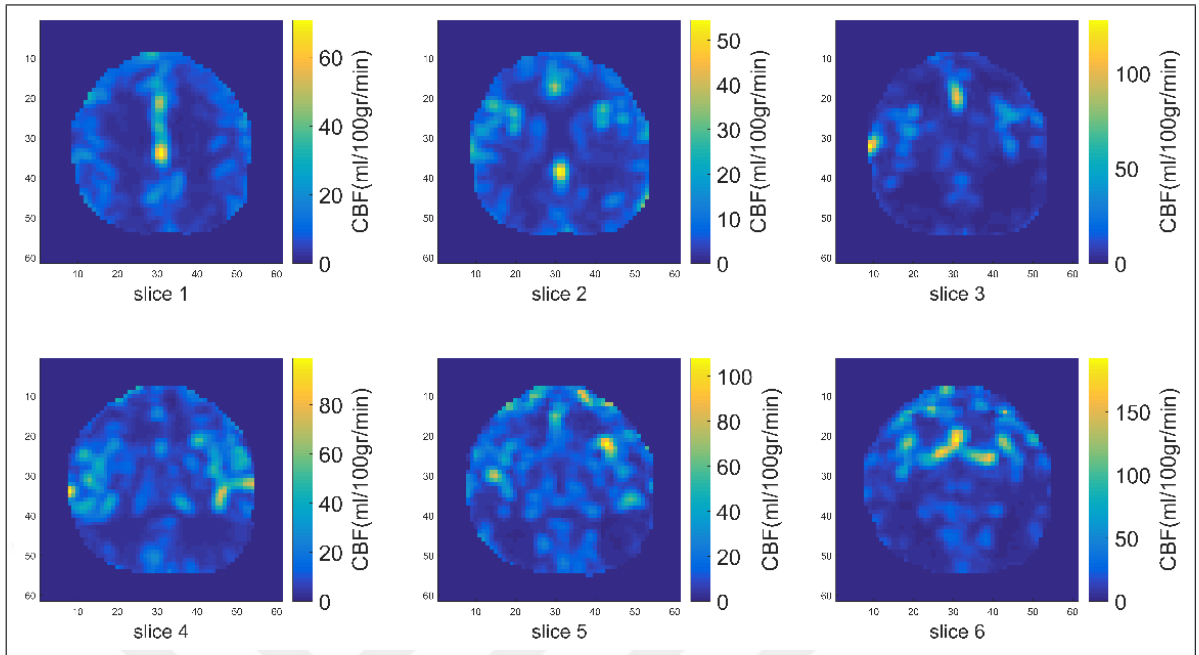


Figure 4.8 CBF maps taken from the 2nd region of a PD-CN patient.

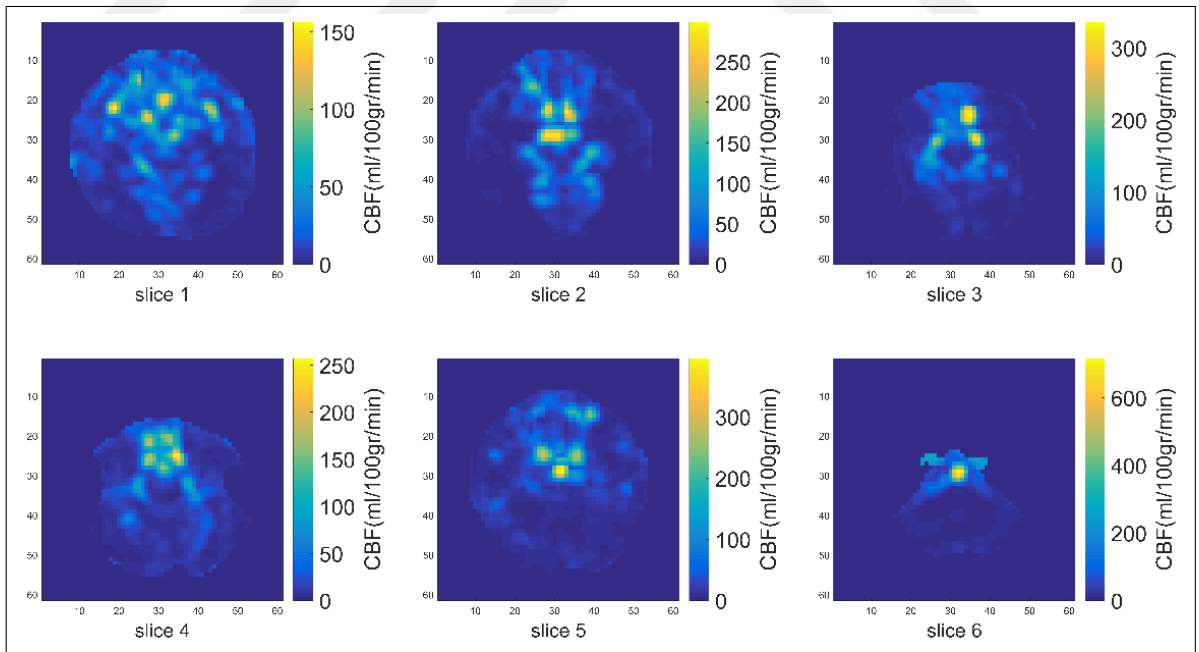


Figure 4.9 CBF maps taken from the 3rd region of a PD-CN patient.

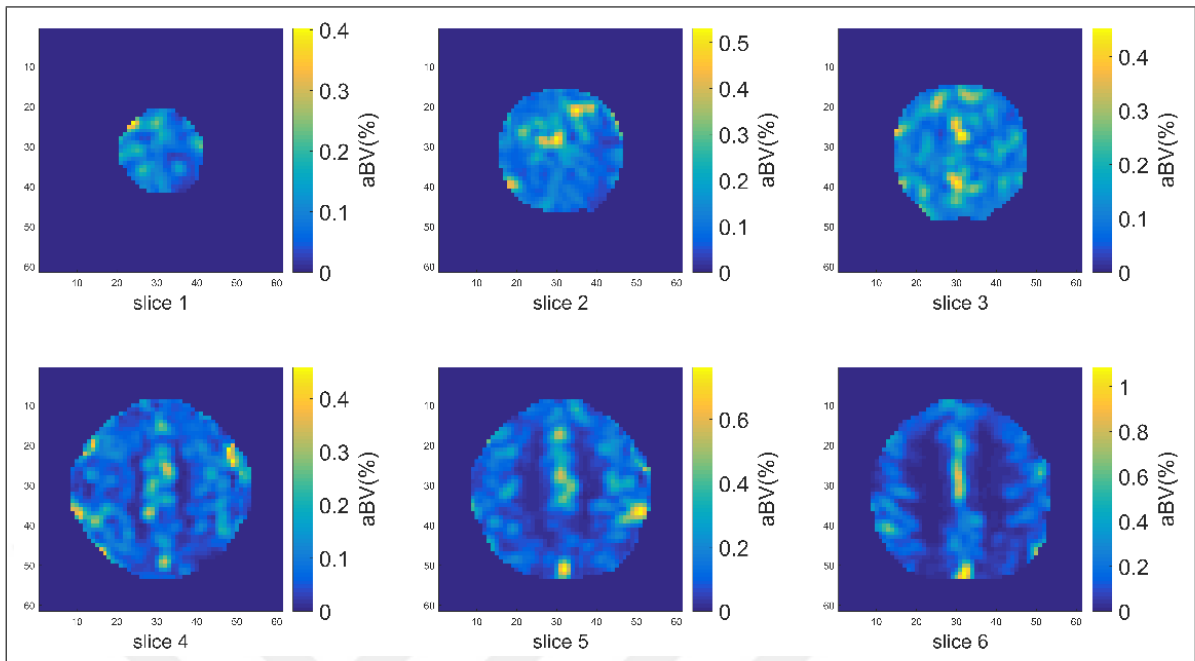


Figure 4.10 aBV maps taken from the 1st region of a PD-CN patient.

4.2 The Mean CBF Value Differences

CBF maps of two patients were not included in the analysis because of head motion. CBF values of PD-MCI patients were compared with that of PD-CN in these regions by using Mann-Whitney ranksum test. In Table 4.1, the mean (\pm std) CBF values in these brain regions can be seen with the corresponding p values. Decreased perfusion was seen in precuneus region in patients with PD-MCI with respect to patients with PD-CN. After Bonferroni multiple comparison correction was applied to adjust p values, there was not any statistically significant difference between the CBF values of PD-MCI and PD-CN patients in any regions.

Table 4.1

The mean CBF values (\pm std) of PD-CN and PD-MCI patients in different brain regions, and the p-values calculated with a Mann-Whitney ranksum test.

	Precuneus	Cingulate Gyrus	Frontal Lobe	Temporal Lobe	Subfrontal Gyrus	Occipital Lobe
PD-CN	62.83 \pm 25.89	68.3 \pm 18.6	63.07 \pm 28.65	58.82 \pm 26.74	72.86 \pm 32.89	37.71 \pm 20.92
PD-MCI	44.2 \pm 16.67	64.58 \pm 22.3	59.29 \pm 23.76	61.02 \pm 25.64	55.73 \pm 26.6	38.39 \pm 20.37
p	0.03*	0.81	0.70	0.75	0.13	0.96

*trend $p < 0.05$. ** $p < 0.05/6$ was considered as statistically significant.

The mean (\pm std) aBV values were calculated in the same brain regions, and were compared between PD-MCI and PD-CN patients by using Mann-Whitney ranksum test. Table 4.2 shows the mean aBV values (\pm std) of PD-MCI and PD-CN patients in different brain regions with p values. As can be seen, there was not any statistically significant difference between the aBV values of the two group of patients in any of the regions.

Table 4.2

The mean aBV values (\pm std) of PD-CN and PD-MCI patients in different brain regions, and the p values calculated with a Mann-Whitney ranksum test.

	Precuneus	Cingulate Gyrus	Frontal Lobe	Temporal Lobe	Subfrontal Gyrus	Occipital
PD-CN	1.41 \pm 1.21	1.79 \pm 1.17	2.20 \pm 1.82	0.1 \pm 0.27	2.82 \pm 2.23	1.27 \pm 1.16
PD-MCI	1.25 \pm 0.76	1.63 \pm 1.3	1.65 \pm 1.36	0.25 \pm 0.9	1.84 \pm 1.63	1.54 \pm 0.72
p	0.91	0.52	0.38	0.76	0.19	0.25

*trend $p < 0.05$. ** $p < 0.05/6$ was considered as statistically significant.

Also, the CBF values of different brain regions were compared with each other in each patient group using a Friedman test. Table 4.3 shows the mean ranks of the CBF values. There was a statistically significant difference between CBF values calculated in these brain regions for both PD-MCI and PD-CN ($p=0.031$, and $p=0.007$, respectively). Afterwards, SNK test was used to determine pairwise CBF value differences between regions. The CBF values were statistically significantly different between cingulate gyrus and occipital lobe for PD-MCI patients. On the other hand, the CBF values were statistically significantly different in cingulate gyrus, occipital lobe, frontal lobe

and subfrontal gyrus for PD-CN patients. There were statistically significant CBF differences between cingulate gyrus and occipital lobe, frontal lobe and occipital lobe, and occipital and subfrontal gyrus.

Table 4.3

The mean rank of CBF values in some brain regions, and p values calculated with a Friedman test.

	PD-MCI	PD-CN
Brain regions	Mean Rank	Mean Rank
Precuneus	2.76	3.58
Cingulate Gyrus	4.18	4.08
Frontal	4.24	3.92
Temporal	3.59	3.77
Subfrontal Gyrus	3.71	4.15
Occipital	2.53	1.69
p	0.031*	0.007*

* $p < 0.05$ was considered as statistically significant.

4.3 Correlation of Neuropsychological Test Scores and CBF Values

Table 4.4 shows the neuropsychological test scores of 19 patients with PD-MCI and 19 patients with PD-CN.

Table 4.5 shows the mean test scores in PD-MCI and PD-CN, and the p-values calculated with a Mann-Whitney ranksum test for testing the difference between patient groups. It was found that there was a statistically significant difference between ACER values ($p < 0.0001$).

Table 4.4
Neuropsychological test scores of PD-MCI and PD-CN patients.

PD-MCI	GDS	UPDRS	ACER	STROOP	LINE	SDMT	PD-CN	GDS	UPDRS	ACER	STROOP	LINE	SDMT
1	7	46	76	57	16	18	1	9	60	84	64	12	16
2	1	22	82	47	25	33	2	11	57	89	69	24	17
3	13	56	72	46	26	31	3	5	32	84	97	27	25
4	10	79	72	60	21	18	4	5	70	90	65	26	24
5	9	74	71	72	18	13	5	9	74	71	72	18	13
6	2	13	68	14	22	18	6	11	53	98	27	27	48
7	9	70	80	54	26	35	7	5	52	90	57	27	45
8	11	33	82	23	25	32	8	8	47	84	39	24	36
9	7	27	79	68	25	28	9	7	27	79	68	25	28
10	7	55	72	86	19	15	10	11	46	84	79	23	27
11	2	30	69	12	18	16	11	11	87	85	49	22	21
12	4	34	76	77	14	18	12	2	45	91	60	14	32
13	7	65	82	93	20	29	13	0	45	92	28	28	35
14	3	51	72	23	21	25	14	4	36	89	39	22	26
15	3	17	75	26	24	35	15	8	38	88	46	22	18
16	2	49	68	55	24	19	16	11	30	95	37	18	26
17	4	66	80	33	13	20	17	4	70	85	48	26	24
18	11	66	66	55	27	15	18	5	56	86	64	20	23
19	10	43	72	67	19	18	19	2	80	87	48	25	24

Table 4.5
The mean test scores values (\pm std) of PD-CN and PD-MCI, and p values calculated with a Mann-Whitney ranksum test.

	PD-MCI	PD-CN	P
GDS	6.42 \pm 3.32	6.58 \pm 3.72	0.73
Line	21.21 \pm 4.2	23.26 \pm 4.6	0.09
Stroop	50.95 \pm 23.9	55.37 \pm 19.17	0.62
UPDRS	47.16 \pm 20.06	52.06 \pm 15.72	0.5
SDMT	22.92 \pm 7.40	27.46 \pm 8.82	0.11
ACER	74.42 \pm 5.18	88.82 \pm 4.14	3.12E-07**

*trend $p < 0.05$. ** $p < 0.05/6$ was considered as statistically significant.

Table 4.6 shows the mean (\pm std) CBF values and correlation coefficient (R) and p values calculated by applying a Spearman rank correlation test. A trend for negative correlations were found between CBF values and GDS in precuneus, UPDRS in occipital lobe, and ACER in subfrontal gyrus for PD-MCI patients.

Table 4.6

The mean test scores (\pm std) in different brain regions, and p values calculated with Spearman rank correlation test.

		Precuneus		Cingulate		Frontal		Subfrontal		Occipital		Temporal	
		PD-MCI	PD -CN	PD-MCI	PD								
ACER	Mean \pm std	74.78 \pm 5.09	88.58 \pm 3.98	74.78 \pm 5.10	88.72 \pm 4.04	74.70 \pm 5.24	88.53 \pm 4.08	74.71 \pm 5.24	98.97 \pm 4.09	74.78 \pm 5.10	88.94 \pm 4.11	74.78 \pm 5.09	88.5 \pm 4.31
	R	0.18	0.41	0.07	-0.11	0.36	-0.45	-0.59	0.23	0.13	0.21	0.23	-0.47
	p	0.48	0.91	0.79	0.65	0.16	0.07	0.01*	0.40	0.61	0.44	0.37	0.09
Stroop	Mean \pm std	53 \pm 22.77	55.37 \pm 19.16	53 \pm 22.77	54.89 \pm 19.6	51.59 \pm 22.65	56.47 \pm 18.98	51.59 \pm 22.65	54 \pm 20.69	53.00 \pm 22.77	54.18 \pm 20.71	53 \pm 22.77	56.8 \pm 20.9
	R	-0.01	-0.29	-0.28	-0.16	0.28	-0.16	-1.36	0.44	-0.25	0.02	-0.15	0.10
	p	0.98	0.23	0.26	0.52	0.28	0.53	0.60	0.09	0.31	0.95	0.56	0.75
Line	Mean \pm std	21.17 \pm 4.31	23.26 \pm 4.59	21.17 \pm 4.31	23.44 \pm 4.65	21.59 \pm 4.04	23.18 \pm 4.65	21.59 \pm 4.05	24.75 \pm 2.84	21.17 \pm 4.31	23.94 \pm 3.94	21.17 \pm 4.31	24 \pm 3.04
	R	-0.28	-0.05	0.23	0.03	0.11	-0.36	0.32	0.29	0.37	-0.23	-0.1	-0.21
	p	0.26	0.83	0.36	0.91	0.68	0.16	0.22	0.27	0.14	0.40	0.69	0.47
SDMT	Mean \pm std	23.22 \pm 7.66	27.42 \pm 9.72	21.17 \pm 4.31	27.67 \pm 2.09	23.53 \pm 7.79	27.23 \pm 8.98	23.53 \pm 7.87	18.12 \pm 8.90	23.22 \pm 7.66	27.31 \pm 7.79	23.22 \pm 7.66	23.36 \pm 7.96
	R	-0.04	-0.15	0.31	-0.24	0.16	-0.34	-0.03	-0.41	0.29	-0.29	0.23	-0.01
	p	0.88	0.54	0.21	0.34	0.54	0.18	0.26	0.12	0.25	0.28	0.38	0.97
UPDRS	Mean \pm std	49.06 \pm 18.80	52.05 \pm 15.72	40.06 \pm 18.80	51.83 \pm 16.15	49.94 \pm 19	52.23 \pm 16.55	49.94 \pm 18.10	51.75 \pm 16.97	49.06 \pm 18.91	51.32 \pm 17.06	49.05 \pm 18.80	50.50 \pm 16.35
	R	-0.36	0.03	-0.26	0.34	0.30	-0.08	0.33	0.19	-0.55	0.11	-0.40	-0.04
	p	0.14	0.91	0.30	0.17	0.26	0.77	0.20	0.47	0.02*	0.68	0.10	0.89
GDS	Mean \pm std	6.67 \pm 3.66	6.58 \pm 3.65	6.67 \pm 7	6.66 \pm 3.74	6.82 \pm 3.71	7.05 \pm 3.45	6.92 \pm 3.71	6.69 \pm 3.79	6.68 \pm 3.66	6.62 \pm 3.91	6.67 \pm 3.66	7.64 \pm 3.18
	R	-0.56	-0.16	-0.23	0.04	-0.04	-0.04	0.03	-0.19	-0.05	0.18	-0.24	0.11
	p	0.02*	0.50	0.35	0.97	0.87	0.89	0.91	0.48	0.95	0.50	0.34	0.72

*trend $p < 0.05$. $p^{**} < 0.05/6$ was considered as statistically significant.

4.4 Histogram

Table 4.7 shows the histogram parameters of CBF values before and after aBV correction and the p value of their differences for a PD-MCI and a PD-CN patient. The skewness, kurtosis and peak height decreased for both patients ($p < 0.001$). The peak position did not statistically significant differed between before and after aBV correction for both patients.

Table 4.7

The histogram analysis of patients in one brain slice, and p values calculated with Wilcoxon signed rank test.

	PD-MCI			PD-CN		
	mean±std		p	mean±std		p
	CBF	CBF_aBV		CBF	CBF_aBV	
Peak height	97.94±42.31	77.76±38.01	2.92e-04*	95.23±61.35	69.35±39.32	0.0012*
Peak position	13.25±2.13	12.18±1.10	0.0113	12.52±1.67	11.75±1.48	0.0168
Kurtosis	12.54±6.46	10.93±5.3	5.03e-4*	12.28±6.38	10.84±5.55	2.93e-04*
Skewness	2.67±0.94	2.46±0.83	5.03e-04*	2.43±0.79	2.62±0.85	3.51e-04*

* $p < 0.006$

Figure 4.11 shows the histogram of one slice before, and Figure 4.12 shows the histogram after aBV correction in a slice of the CBF map for the PD-CN patient. The range of the values of the CBF map were [10, 100] before, and [10, 80] after the aBV correction.

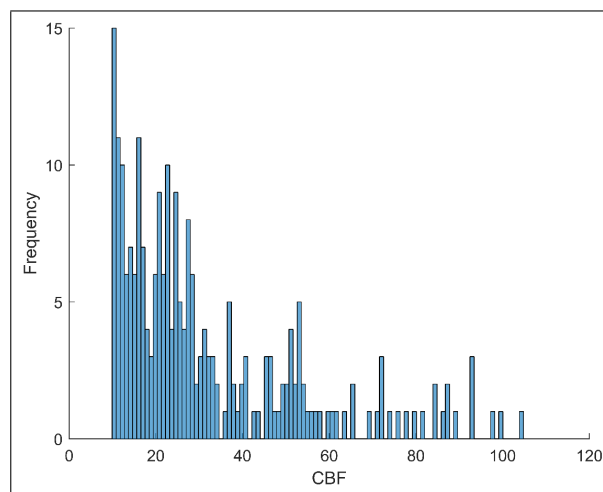


Figure 4.11 The histogram of a CBF map calculated without aBV correction.

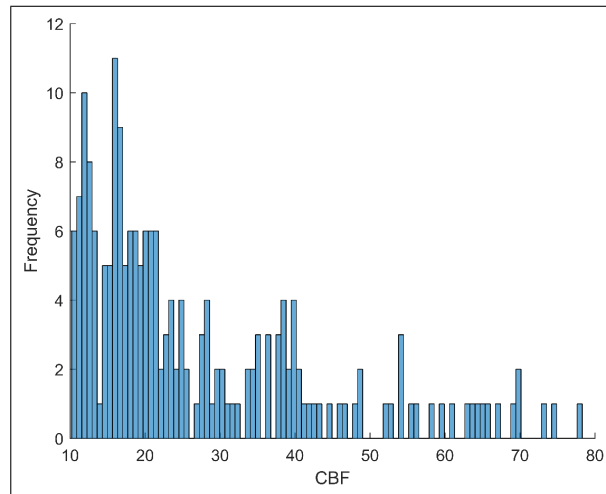


Figure 4.12 The histogram of a CBF map calculated with aBV correction.

5. DISCUSSION

The results of our study are consistent with previous studies measuring perfusion by SPECT in PD-MCI and PD-CN patients. These studies showed subtle perfusion changes in parieto-occipital regions in PD-MCI patients compared with PD-CN patients [46]. There were not any statistically significant differences between any brain regions in PD-MCI patients compared to PD-CN patients in our study. However, there was a trend of decreased perfusion in the precuneus in PD-MCI patients. The decreased perfusion in precuneus in patients with PD-MCI relative to PD-CN might be related to cognitive, visual and sensorimotor deficits, because decreased perfusion in neurodegenerative diseases has been attributed to either tissue loss or functional connectivity loss [47, 48]. The mean aBV values were not statistically significantly different between patient groups.

There was a trend for a negative correlation between the CBF values in the precuneus and GDS scores in the PD-MCI patients. GDS score increases in depression, and CBF decrease in several regions of PD-MCI patients might be related with it. On the other hand, a trend for a negative correlation was found between ACER and CBF values of PD-MCI patients in subfrontal gyrus. Previous studies found a reduction of CBF values of PD-MCI patients in subfrontal gyrus with respect to PD-CN patients and HC [7, 8, 9]. Additionally, increase in ACER scores shows better cognitive functioning [49], and PD-MCI diagnosis is mainly made based on the reduction of ACER scores. Therefore, the correlation between CBF values in subfrontal gyrus and ACER was expected to be positive, and our findings require further analysis. Additionally, a negative trend was found between UPDRS and CBF values in PD-MCI. UPDRS increases with cognitive impairment, and CBF decrease in PD-MCI patients in several regions might be related with cognitive impairment.

In the current study, we found changes in histogram patterns of CBF values derived from ASL-MRI images after aBV correction. The skewness values of CBF

histograms calculated with and without aBV correction were positive, which meant that distributions were skewed right. Additionally, kurtosis decreased after aBV correction, which meant lower peaks. The decrease in skewness and kurtosis meant that the CBF distributions were closer to normal and the value of high peaks decreased. Therefore, the distribution of CBF values obtained from patients was closer to normal after aBV correction. Changes in PP and PH were detected in all patients. There was a statistically significant difference in PH, whereas there was not a statistically significant difference in PP. The decrease in PH was due to the reduction of the arterial blood signal. Also, aBV correction didn't affect the position of the main peak in CBF histograms.

There are two different analysis techniques for estimating CBF values in brain regions. These are registration and region of interest analysis [44]. There have not been any studies calculating CBF values after registration into a brain atlas in PD patients. In general, ROI was used to estimate CBF values in PD [7, 8, 9]. In ROI analysis, the regions of CBF maps are visually determined. The disadvantage of this technique is that the ROI definition is somewhat subjective, which could cause incorrect estimation of the CBF values. And, it would be quite time consuming to define several brain regions by hand.

Several of the previous ASL-MRI studies done on other MR vendors used the scanner software to calculate CBF maps. However, available software had some drawbacks, one of which is that main magnetization was taken as constant, which might have resulted in wrong CBF estimation, because main magnetization is different in each control image. In Philips MR system, control, tag, and the subtraction of these images are acquired. In our study, main magnetization was estimated from multi TI ASL-MRI data, and CBF maps were calculated by taking into account M_0 variations. Also, another drawback of the previous studies was the limited number of subjects [7, 8, 9].

However, some limitations of our study should be noted. We did not include healthy controls. Additionally, the brain location of some patients in head coil changed

after T2w images were acquired. Therefore, these patients were excluded from the study. CBF maps have low resolution, which was a problem in registration, and CBF values in some brain regions could not be estimated. Also, there were some artifacts in ASL-MR images, which might have had a negative effect on estimating CBF values.

The ASL-MRI technique could provide clinicians and researchers with an attractive alternative to radiotracer methods in many aspects including safety, availability, repeatability, cost and effectiveness. Using 3T MRI scanner is preferable for ASL-MRI technique, since high field provides higher signal to noise. But, acquisition of ASL-MRI at 1.5T MRI scanners is also feasible, which are more widespread over the world [50]. CBF maps might offer an easily applicable biomarker that may be useful for future longitudinal investigations and assessment of PD progression.

6. CONCLUSION

To our knowledge, this is the first comprehensive study comparing the CBF maps of PD-MCI and PD-CN using ASL-MRI in the literature. Relative cerebral perfusion differences in PD-MCI patients might serve as potential biomarkers of cognitive impairment in PD patients. Also, we identified negative correlation trends between CBF values and neuropsychological test scores indicating cognitive impairment might be related with perfusion deficits in the brain. In future studies, the population of PD-MCI and PD-CN will be increased, and healthy controls will be included in our study. Also, the same subjects will be scanned after 1.5 years, and the CBF maps will be compared to identify possible biomarkers, which might indicate a conversion from PD-MCI to PDD. Additionally, other ASL sequences might be implemented for creating better CBF maps.

APPENDIX A. Software Packages

1. FSL (<http://fsl.fmrib.ox.ac.uk/fsl/fslwiki/>),
2. MATLAB (<http://www.mathworks.com/downloads/>).



REFERENCES

1. Brooks, D. J., K. A. Frey, K. L. Marek, D. Oakes, D. Paty, R. Prentice, C. W. Shults, and A. J. Stoessl, "Assessment of neuroimaging techniques as biomarkers of the progression of parkinson's disease," *Exp Neurol*, Vol. 184 Suppl 1, pp. S68–79, 2003.
2. Wong, E. C., R. B. Buxton, and L. R. Frank, "Implementation of quantitative perfusion imaging techniques for functional brain mapping using pulsed arterial spin labeling," *NMR Biomed*, Vol. 10, no. 4-5, pp. 237–49, 1997.
3. Williams, D. S., J. A. Detre, J. S. Leigh, and A. P. Koretsky, "Magnetic resonance imaging of perfusion using spin inversion of arterial water," *Proc Natl Acad Sci U S A*, Vol. 89, no. 1, pp. 212–6, 1992.
4. Buxton, R. B., L. R. Frank, E. C. Wong, B. Siewert, S. Warach, and R. R. Edelman, "A general kinetic model for quantitative perfusion imaging with arterial spin labeling," *Magn Reson Med*, Vol. 40, no. 3, pp. 383–96, 1998.
5. Wong, E. C., R. B. Buxton, and L. R. Frank, "Quantitative imaging of perfusion using a single subtraction (quips and quips ii)," *Magn Reson Med*, Vol. 39, no. 5, pp. 702–8, 1998.
6. Petersen, E. T., T. Lim, and X. Golay, "Model-free arterial spin labeling quantification approach for perfusion mri," *Magn Reson Med*, Vol. 55, no. 2, pp. 219–32, 2006.
7. Melzer, T. R., R. Watts, M. R. MacAskill, J. F. Pearson, S. Rueger, T. L. Pitcher, L. Livingston, C. Graham, R. Keenan, A. Shankaranarayanan, D. C. Alsop, J. C. Dalrymple-Alford, and T. J. Anderson, "Arterial spin labelling reveals an abnormal cerebral perfusion pattern in parkinson's disease," *Brain*, Vol. 134, no. Pt 3, pp. 845–55, 2011.
8. Le Heron, C. J., S. L. Wright, T. R. Melzer, D. J. Myall, M. R. MacAskill, L. Livingston, R. J. Keenan, R. Watts, J. C. Dalrymple-Alford, and T. J. Anderson, "Comparing cerebral perfusion in alzheimer's disease and parkinson's disease dementia: an asl-mri study," *J Cereb Blood Flow Metab*, Vol. 34, no. 6, pp. 964–70, 2014.
9. Chao, L. L., S. T. Buckley, J. Kornak, N. Schuff, C. Madison, K. Yaffe, B. L. Miller, J. H. Kramer, and M. W. Weiner, "Asl perfusion mri predicts cognitive decline and conversion from mci to dementia," *Alzheimer Dis Assoc Disord*, Vol. 24, no. 1, pp. 19–27, 2010.
10. Campbell, A. M., and C. Beaulieu, "Comparison of multislice and single-slice acquisitions for pulsed arterial spin labeling measurements of cerebral perfusion," *Magn Reson Imaging*, Vol. 24, no. 7, pp. 869–76, 2006.
11. Pagonabarraga, J., and J. Kulisevsky, "Cognitive impairment and dementia in parkinson's disease," *Neurobiol Dis*, Vol. 46, no. 3, pp. 590–6, 2012.
12. Louis, E. D., "The shaking palsy, the first forty-five years: a journey through the british literature," *Mov Disord*, Vol. 12, no. 6, pp. 1068–72, 1997.
13. de Lau, L. M., and M. M. Breteler, "Epidemiology of parkinson's disease," *Lancet Neurol*, Vol. 5, no. 6, pp. 525–35, 2006.
14. Jankovic, J., "Parkinson's disease: clinical features and diagnosis," *J Neurol Neurosurg Psychiatry*, Vol. 79, no. 4, pp. 368–76, 2008.

15. Fearnley, J. M., and A. J. Lees, "Ageing and parkinson's disease: substantia nigra regional selectivity," *Brain*, Vol. 114 (Pt 5), pp. 2283–301, 1991.
16. Korczyn, A. D., "Mild cognitive impairment in parkinson's disease," *J Neural Transm (Vienna)*, Vol. 120, no. 4, pp. 517–21, 2013.
17. Liu, T. T., and G. G. Brown, "Measurement of cerebral perfusion with arterial spin labeling: Part 1. methods," *J Int Neuropsychol Soc*, Vol. 13, no. 3, pp. 517–25, 2007.
18. Alsop, D. C., J. A. Detre, X. Golay, M. Gunther, J. Hendrikse, L. Hernandez-Garcia, H. Lu, B. J. MacIntosh, L. M. Parkes, M. Smits, M. J. van Osch, D. J. Wang, E. C. Wong, and G. Zaharchuk, "Recommended implementation of arterial spin-labeled perfusion mri for clinical applications: A consensus of the ismrm perfusion study group and the european consortium for asl in dementia," *Magn Reson Med*, Vol. 73, no. 1, pp. 102–16, 2015.
19. Zierler, K. L., "Theoretical basis of indicator-dilution methods for measuring flow and volume," *Circulation Research*, Vol. 10, no. 3, pp. 393–407, 1962.
20. Borogovac, A., and I. Asllani, "Arterial spin labeling (asl) fmri: advantages, theoretical constrains, and experimental challenges in neurosciences," *Int J Biomed Imaging*, Vol. 2012, p. 818456, 2012.
21. Petcharunpaisan, S., J. Ramalho, and M. Castillo, "Arterial spin labeling in neuroimaging," *World J Radiol*, Vol. 2, no. 10, pp. 384–98, 2010.
22. Edelman, R. R., B. Siewert, D. G. Darby, V. Thangaraj, A. C. Nobre, M. M. Mesulam, and S. Warach, "Qualitative mapping of cerebral blood flow and functional localization with echo-planar mr imaging and signal targeting with alternating radio frequency," *Radiology*, Vol. 192, no. 2, pp. 513–20, 1994.
23. Kim, S. G., "Quantification of relative cerebral blood flow change by flow-sensitive alternating inversion recovery (fair) technique: application to functional mapping," *Magn Reson Med*, Vol. 34, no. 3, pp. 293–301, 1995.
24. Pollock, J. M., H. Tan, R. A. Kraft, C. T. Whitlow, J. H. Burdette, and J. A. Maldjian, "Arterial spin-labeled mr perfusion imaging: clinical applications," *Magn Reson Imaging Clin N Am*, Vol. 17, no. 2, pp. 315–38, 2009.
25. Ferre, J. C., E. Bannier, H. Raoult, G. Mineur, B. Carsin-Nicol, and J. Y. Gauvrit, "Arterial spin labeling (asl) perfusion: techniques and clinical use," *Diagn Interv Imaging*, Vol. 94, no. 12, pp. 1211–23, 2013.
26. Pruessmann, K. P., M. Weiger, M. B. Scheidegger, and P. Boesiger, "Sense: sensitivity encoding for fast mri," *Magn Reson Med*, Vol. 42, no. 5, pp. 952–62, 1999.
27. Griswold, M. A., P. M. Jakob, R. M. Heidemann, M. Nittka, V. Jellus, J. Wang, B. Kiefer, and A. Haase, "Generalized autocalibrating partially parallel acquisitions (grappa)," *Magn Reson Med*, Vol. 47, no. 6, pp. 1202–10, 2002.
28. Deshmane, A., V. Gulani, M. A. Griswold, and N. Seiberlich, "Parallel mr imaging," *J Magn Reson Imaging*, Vol. 36, no. 1, pp. 55–72, 2012.
29. Nishimura, D. G., *Principles of Magnetic Resonance Imaging*, Stanford, CA : Stanford University.

30. Look, D. C., "Time saving in measurement of nmr and epr relaxation times," *Review of Scientific Instruments*, Vol. 41, no. 2, p. 250, 1970.
31. Gowland, P., and P. Mansfield, "Accurate measurement of t1 in vivo in less than 3 seconds using echo-planar imaging," *Magn Reson Med*, Vol. 30, no. 3, pp. 351–4, 1993.
32. Gunther, M., M. Bock, and L. R. Schad, "Arterial spin labeling in combination with a look-locker sampling strategy: inflow turbo-sampling epi-fair (its-fair)," *Magn Reson Med*, Vol. 46, no. 5, pp. 974–84, 2001.
33. Calamante, F., S. R. Williams, N. van Bruggen, K. K. Kwong, and R. Turner, "A model for quantification of perfusion in pulsed labelling techniques," *NMR Biomed*, Vol. 9, no. 2, pp. 79–83, 1996.
34. Chappell, M. A., B. J. MacIntosh, M. J. Donahue, M. Gunther, P. Jezzard, and M. W. Woolrich, "Separation of macrovascular signal in multi-inversion time arterial spin labelling mri," *Magn Reson Med*, Vol. 63, no. 5, pp. 1357–65, 2010.
35. Golay, X., E. T. Petersen, and F. Hui, "Pulsed star labeling of arterial regions (pulsar): a robust regional perfusion technique for high field imaging," *Magn Reson Med*, Vol. 53, no. 1, pp. 15–21, 2005.
36. Ishizaki, J., H. Yamamoto, T. Takahashi, M. Takeda, M. Yano, and M. Mimura, "Changes in regional cerebral blood flow following antidepressant treatment in late-life depression," *Int J Geriatr Psychiatry*, Vol. 23, no. 8, pp. 805–11, 2008.
37. Duckrow, R. B., "Regional cerebral blood flow during spreading cortical depression in conscious rats," *J Cereb Blood Flow Metab*, Vol. 11, no. 1, pp. 150–4, 1991.
38. Perlmutter, J. S., "Assessment of parkinson disease manifestations," *Curr Protoc Neurosci*, Vol. Chapter 10, p. Unit10 1, 2009.
39. Stroop, J. R., "Studies of interference in serial verbal reactions (reprinted from journal experimental-psychology, vol 18, pg 643-662, 1935)," *Journal of Experimental Psychology-General*, Vol. 121, no. 1, pp. 15–23, 1992.
40. Kohli, A., and M. Kaur, "Wisconsin card sorting test: Normative data and experience," *Indian J Psychiatry*, Vol. 48, no. 3, pp. 181–4, 2006.
41. Calamia, M., K. Markon, N. L. Denburg, and D. Tranel, "Developing a short form of benton's judgment of line orientation test: an item response theory approach," *Clin Neuropsychol*, Vol. 25, no. 4, pp. 670–84, 2011.
42. Van Schependom, J., M. B. D'hooghe, K. Cleynhens, M. D'hooge, M. C. Haelewyck, J. De Keyser, and G. Nagels, "The symbol digit modalities test as sentinel test for cognitive impairment in multiple sclerosis," *European Journal of Neurology*, Vol. 21, no. 9, pp. 1219–+, 2014.
43. Mioshi, E., K. Dawson, J. Mitchell, R. Arnold, and J. R. Hodges, "The addenbrooke's cognitive examination revised (ace-r): a brief cognitive test battery for dementia screening," *International Journal of Geriatric Psychiatry*, Vol. 21, no. 11, pp. 1078–1085, 2006.
44. Basser, P. J., and C. Pierpaoli, "A simplified method to measure the diffusion tensor from seven mr images," *Magn Reson Med*, Vol. 39, no. 6, pp. 928–34, 1998.

45. Baek, H. J., H. S. Kim, N. Kim, Y. J. Choi, and Y. J. Kim, "Percent change of perfusion skewness and kurtosis: a potential imaging biomarker for early treatment response in patients with newly diagnosed glioblastomas," *Radiology*, Vol. 264, no. 3, pp. 834–43, 2012.
46. Nobili, F., G. Abbruzzese, S. Morbelli, R. Marchese, N. Girtler, B. Dessi, A. Brugnolo, C. Canepa, G. C. Drosos, G. Sambuceti, and G. Rodriguez, "Amnesic mild cognitive impairment in parkinson's disease: a brain perfusion spect study," *Mov Disord*, Vol. 24, no. 3, pp. 414–21, 2009.
47. Borghammer, P., M. Chakravarty, K. Y. Jonsdottir, N. Sato, H. Matsuda, K. Ito, Y. Arahata, T. Kato, and A. Gjedde, "Cortical hypometabolism and hypoperfusion in parkinson's disease is extensive: probably even at early disease stages," *Brain Struct Funct*, Vol. 214, no. 4, pp. 303–17, 2010.
48. Yoshiura, T., A. Hiwatashi, T. Noguchi, K. Yamashita, Y. Ohyagi, A. Monji, E. Nagao, H. Kamano, O. Togao, and H. Honda, "Arterial spin labelling at 3-t mr imaging for detection of individuals with alzheimer's disease," *Eur Radiol*, Vol. 19, no. 12, pp. 2819–25, 2009.
49. Yoshida, H., S. Terada, H. Honda, Y. Kishimoto, N. Takeda, E. Oshima, K. Hirayama, O. Yokota, and Y. Uchitomi, "Validation of the revised addenbrooke's cognitive examination (ace-r) for detecting mild cognitive impairment and dementia in a japanese population," *Int Psychogeriatr*, Vol. 24, no. 1, pp. 28–37, 2012.
50. Alsop, D. C., J. A. Detre, and M. Grossman, "Assessment of cerebral blood flow in alzheimer's disease by spin-labeled magnetic resonance imaging," *Ann Neurol*, Vol. 47, no. 1, pp. 93–100, 2000.